

SURFACE MODIFICATION ON ZLH-DS-ISO NANOCOMPOSITE FOR CONTROLLED RELEASE AND KINETIC BEHAVIOUR OF ISOPROCARB ANION

Zuhailimuna Muda
Norhayati Hashim
Norlaili Abu Bakar
Illyas Md Isa
Wan Rusmawati Wan Mahamod
Sharifah Norain Mohd Sharif
Suriani Abu Bakar
Mazidah Mamat
Syazwan Afif Mohd Zobir
Rahadian Zainul

DOI: <https://doi.org/10.37178/ca-c.21.5.085>

Zuhailimuna Muda, Department of Chemistry, Faculty of Science and Mathematics, Universiti Pendidikan Sultan Idris, 35900 Tanjong Malim, Perak, Malaysia

Norhayati Hashim, Department of Chemistry, Faculty of Science and Mathematics, Universiti Pendidikan Sultan Idris, 35900 Tanjong Malim, Perak, Malaysia.

Nanotechnology Research Centre, Faculty of Science and Mathematics, Universiti Pendidikan Sultan Idris, 35900 Tanjong Malim, Perak, Malaysia.

Email: norhayati.hashim@fsmt.upsi.edu.my

Norlaili Abu Bakar, Department of Chemistry, Faculty of Science and Mathematics, Universiti Pendidikan Sultan Idris, 35900 Tanjong Malim, Perak, Malaysia

Illyas Md Isa, Department of Chemistry, Faculty of Science and Mathematics, Universiti Pendidikan Sultan Idris, 35900 Tanjong Malim, Perak, Malaysia.

Nanotechnology Research Centre, Faculty of Science and Mathematics, Universiti Pendidikan Sultan Idris, 35900 Tanjong Malim, Perak, Malaysia

Wan Rusmawati Wan Mahamod, Department of Chemistry, Faculty of Science and Mathematics, Universiti Pendidikan Sultan Idris, 35900 Tanjong Malim, Perak, Malaysia

Sharifah Norain Mohd Sharif, Department of Chemistry, Faculty of Science and Mathematics, Universiti Pendidikan Sultan Idris, 35900 Tanjong Malim, Perak, Malaysia

Suriani Abu Bakar, Nanotechnology Research Centre, Faculty of Science and Mathematics, Universiti Pendidikan Sultan Idris, 35900 Tanjong Malim, Perak, Malaysia

Department of Physics, Faculty of Science and Mathematics, Universiti Pendidikan Sultan Idris, 35900 Tanjong Malim, Perak, Malaysia

Abstract

A nanocomposite is a material with a nanoscopic size of 10^{-9} m formed from a combination of two or more different materials that have the properties of blended materials. Surface modification of zinc layered hydroxide-dodecyl sulphate-isoprocarb (ZLH-DS-ISO) nanocomposite with chitosan and cellulose acetate was studied, and so is their release behaviour. A powder X-ray diffraction (PXRD) pattern for the intercalation peak showed a d-spacing value of 3.31 nm for both ZLH-DS-ISO nanocomposites coated with chitosan and cellulose acetate. The FTIR spectra of coated nanocomposites showed the existence of both chitosan and cellulose acetate. The controlled release of ISO from ZLH-DS-ISO nanocomposite coated with chitosan showed slow release compared to ZLH-DS-ISO nanocomposite coated with cellulose acetate. The kinetic behaviour of ISO from ZLH-DS-ISO nanocomposite coated with chitosan is governed by first-order for Na_3PO_4 solution and parabolic diffusion for both Na_2SO_4 and NaCl solutions. Meanwhile, the kinetic behaviour of ISO anion from ZLH-DS-ISO nanocomposite coated with cellulose acetate follows a pseudo-second-order for all Na_3PO_4 , Na_2SO_4 and NaCl solutions. These polymeric coated nanocomposites, consisting of organic-inorganic nanolayers, showed enhanced release performance compared to uncoated nanocomposites. This study will be beneficial in promoting a good work environment by ensuring the safer use of insecticide by workers and users.

Keywords: Nanocomposite; controlled release formulation; chitosan; cellulose acetate; surface modification

Introduction

Surface modification of organic-inorganic nanocomposites has attracted a lot of attention because it offers an interesting integration and improved interface between nanoparticles and other matrices[1-5]. [1] Lallo et al. used (3-glycidyloxypropyl) trimethoxysilane as a surface coater for ZnO, and the results showed that the smaller ZnO nanoparticle had better antibacterial activity. To modify nanomaterials and nanoparticles, inorganic metals such as silica and noble metals, small organic molecules such as citric and oleic acid, and organic polymers such as chitosan and dextran were used[6]. Among them, polymeric nanocomposites have been widely studied in controlled release applications. Dextran, chitosan, carboxymethyl cellulose, ethyl cellulose, poly(ethylenimine), and poly(ethylene glycol) are common polymers used as coating material[7-11]. Above all, chitosan is often chosen due to its biocompatible and biodegradable natural polymer, which forms a viscous liquid when solubilized in acid. Moreover, because of its abundant source and low price, it is suitable for commercial applications[12-14].

Polymer coating materials for pesticides are commonly applied in controlled release formulations. Biodegradation of polymer coating materials is one of the factors applicable in pesticide release throughout a growing season[15]. A coated pesticide with polymer will immobilize the agrochemical product and make it resistant to runoff and leaching. A coated pesticide also protects the pesticide from environmental degradation such as microorganisms or chemical reactions. This will extend the amount of time it takes the plant to absorb the agrochemicals [16-18]. Chitosan, a natural biodegradable copolymer of N-acetylglucosamine, has been selected as a coating material owing to its cost-effectiveness, biocompatibility, non-toxic, degradation product, and non-carcinogenicity[19, 20]. This copolymer can easily be used to make a variety of products in the agro-industry [21-24]. While, cellulose acetate (CA) is a synthetic polymer used as a membrane material and an attractive

material due to its low cost of production, biodegradability, and non-toxic properties, which have numerous applications in agriculture and horticulture. The type of coating materials affects the release behaviour and dissolution rates of water-soluble pesticides from the host[25-27]. Therefore, this research aims to study the release behaviour of isoprocarb insecticide anion from the polymeric nanocomposites to sustain the release of insecticides into the media. The surface modification of ZLH-DS-ISO nanocomposite using chitosan/cellulose acetate would be ideal for slow-release formulation and is believed to be crucial for the continued good agricultural practice in plant cultivation.

Experimental

2.1 Synthesis of ZLH-DS-ISO nanocomposites coated with chitosan

As previously described, a ZLH-DS-ISO nanocomposite was prepared in advance[28]. A ZLH-insecticide-coated chitosan nanocomposite was synthesized by the self-assembly method [29, 30]. This nanocomposite was prepared as follows: 0.1 g of chitosan was dissolved in 50 mL of 1% acetic acid solution. The mixture of chitosan solution and 0.1 g of nanocomposite was stirred for 18 hours. The precipitated nanocomposite was washed by repeated cycles of centrifugation. The chitosan-coated nanocomposite was dried for 24 hours in an oven at 60 °C and kept in a sample bottle.

2.2 Synthesis of ZLH-DS-ISO nanocomposite coated with cellulose acetate

The cellulose acetate (CA) coating was done by the modification method as described in previous studies[31, 32]. The CA solution was prepared by dissolving 0.1 g of CA in 25 mL of acetone. The 0.1 g of pesticide nanocomposite granules were placed in the CA solution and stirred for 18 hours. The coated granules were centrifuged and dried at 60 °C. The final product, designated as a CA-coated pesticide nanocomposite, was obtained.

2.3 Characterization of layered material nanocomposites

Several instruments have been used to characterize the synthesized ZLH nanocomposites. The PXRD patterns were obtained using Bruker AXS power diffraction (D8 Advance, $\lambda = 1.5406 \text{ \AA}$, $\text{CuK}\alpha = 60 \text{ kV}$ and 60 mA , $2\theta = 2^\circ$ to 60° at 2° min^{-1}). The FTIR spectra were obtained using Thermo Nicolet 6700 FTIR (KBr pellet) at a range of $400\text{--}4000 \text{ cm}^{-1}$. Thermal stability analysis was obtained using Perkin Elmer Pyris 1 TGA Thermo (heating rate = $20^\circ\text{C min}^{-1}$). The surface morphology analysis was performed using FESEM (Hitachi model SU 8020 UHR).

2.4 Controlled release study of insecticide

Solutions of Na_3PO_4 , Na_2SO_4 , and NaCl were prepared at various concentrations (0.10 M, 0.20 M, and 0.30 M). The release medium was chosen because of its presence in rainwater and soil composition[33, 34]. The cuvette was filled with 0.6 mg nanocomposites[35], and the release of isoprocarb anion was measured at the preset time at $\text{max} = 270.0 \text{ nm}$.

Results and Discussion

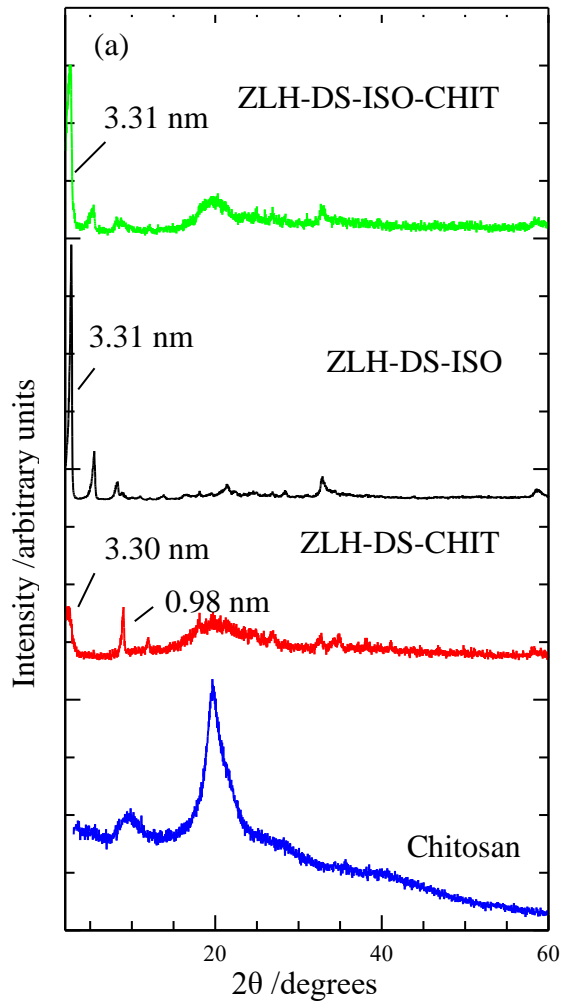
3.1 The PXRD pattern analysis

Figure 1 (a) shows the PXRD pattern of ZLH-DS-ISO-CHIT (zinc layered hydroxide-dodecyl sulphate-isoprocarb-chitosan) nanocomposites. A nanocomposite of 0.0025 M isoprocarb with high crystallinity was chosen to be coated with chitosan.

The intercalation peak for both coated and uncoated ZLH-DS-ISO was centred at 3.31 nm. The coated host (ZLH-DS-CHIT) has basal spacing at 3.30 nm and 0.98 nm, due to previously reported $Zn_5(OH)_8(NO_3)_2 \cdot 2H_2O$ [36, 37]. A broad peak around 20° at a 2θ angle also appeared in both coated ZLH-DS and ZLH-DS-ISO nanocomposites, which corresponded to the superimposed peak of the coating material, chitosan [38]. Chitosan was coated onto the surface of both ZLH-DS and ZLH-DS-ISO nanocomposites via hydrogen bonding of $-OH$ groups in ZLH and also $-OH$ and $-NH_2$ groups in chitosan, which was similar to the interaction reported by previous studies [39-41].

The ZLH-DS-ISO-CA (zinc layered hydroxide-dodecyl sulphate-isopropyl cellulose acetate) nanocomposite PXRD pattern is shown in Figure 1 (b). An uncoated nanocomposite of 0.0025 M isopropyl cellulose acetate (CA), similar to the chitosan-coated nanocomposite. The intercalation peak for both coated and uncoated ZLH-DS-ISO nanocomposite was 3.31 nm. The coated host ZLH-DS-CA had a basal spacing of 3.30 nm, and the second peak with a value of 0.98 nm corresponds to $Zn_5(OH)_8(NO_3)_2 \cdot 2H_2O$. A wide peak around 20° was also found in the ZLH-DS-CA and ZLH-DS-ISO-CA nanocomposites, corresponding to the superimposed CA peak. The presence of a hydrogen bond between the hydroxyl group of CA and the ZLH layers is critical for the coating process [42, 43].

The result showed that there was no significant change in d-spacing values for all coated hosts, ZLH-DS, and ZLH-DS-ISO nanocomposites after coating with chitosan and CA [44], proposed that the cellulose acetate molecule adsorbed on the surface of the ZLH particles during the coating process is not exchanged with the anion inside the layer. The intensity peak of both ZLH-DS-ISO-CHIT and ZLH-DS-ISO-CA nanocomposites was slightly decreased compared to the uncoated one, which was due to the disorder of stacked metal hydroxide layers [45]. A similar observation was also reported for polymer coatings on the surface of layered materials [45-50]. Additionally, there was a considerable broadening of the diffraction peaks upon coating the chitosan and CA matrix. This broadening was frequently associated with a reduction in the particle size of the crystallites or turbostratic of the layers, resulting in irregular or mismatched stacking of sequential layers [51].



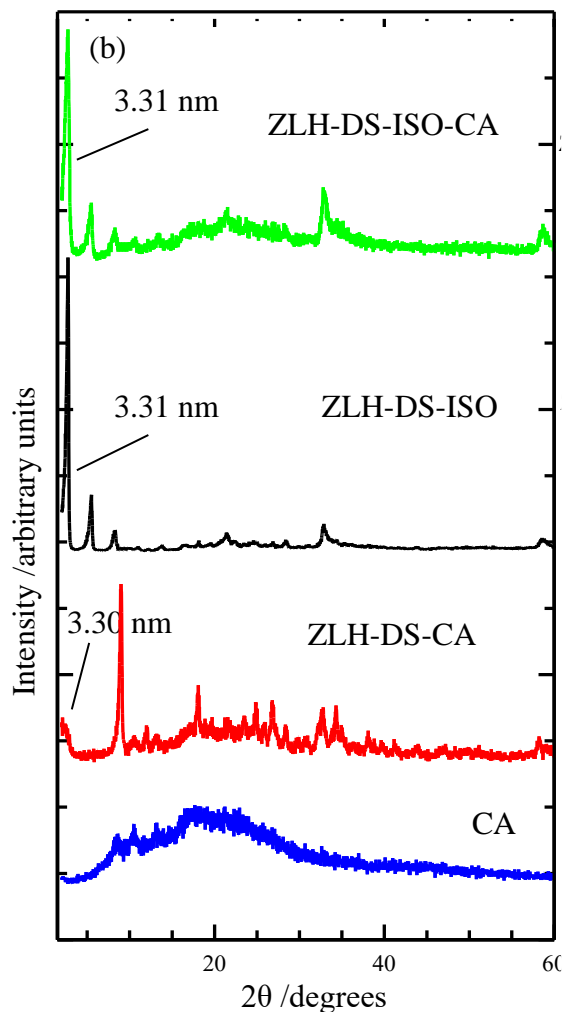


Figure 1 PXR D pattern of chitosan (a) and cellulose acetate (b) coated nanocomposites.

3.2 FTIR spectroscopy

Figure 2 shows the FTIR spectra of chitosan, uncoated and coated nanocomposites. As shown in Figure 2, chitosan-coated ZLH-DS showed a strong absorption peak at 3312 cm^{-1} , which corresponded to the stretching vibrations of the hydroxyl group of free water molecule[52]. Two doublet absorption peaks at 2846 cm^{-1} and 2913 cm^{-1} indicated the presence of stretching vibration for the aliphatic group of CH_2 . The absorption peak of the interlayer water molecule was overlaid with the bending vibration of the N-H group, which was centred at 1635 cm^{-1} . Whereas, peaks at 1216 cm^{-1} and 1379 cm^{-1} indicated the existing sulphate group in SDS and the NO_3^- group from zinc nitrate, respectively[52, 53]. An adsorption peak at 1379 cm^{-1} that was overlaid with an adsorption peak of nitrate supported the presence of chitosan in ZLH-DS spectra.

The coated nanocomposite, ZLH-DS-ISO-CHIT, exhibits an adsorption band similar to both the ZLH-DS-CHIT and the chitosan spectra. All three adsorption peaks at 3312 cm^{-1} , 2913 cm^{-1} , and 2846 cm^{-1} exactly resemble the ZLH-DS-CHIT peak, which is attributed to the OH group and sp^3 stretching of the C-H group. The bending vibration of N-H that disappeared after the intercalation of isoproc carb reappeared at 1714 cm^{-1} referring to the presence of N-H group in chitosan molecule and the sp^3 C-H bending vibration peak centred at 1439 cm^{-1} and 1532 cm^{-1} . Whereas the peak centred at 1258 cm^{-1} was due to C-N stretching vibration. The symmetric and asymmetric stretching vibrations of S=O from SDS molecule[54] correspond to the peaks at 1086 cm^{-1} and 1216 cm^{-1} .

Four main absorptions were highlighted in the FTIR spectra of chitosan. The peak that appeared at 3427 cm^{-1} was due to the hydroxyl stretching vibration group, which also overlapped with the peak of N-H stretching vibration. In contrast, the N-H bending vibration group occurred at 1640 cm^{-1} . The stretching vibration peak of C-H[55] was observed at 2918 cm^{-1} whereas the stretching vibration of the C-N group was present at 1379 cm^{-1} . Table 1 shows the main peaks for ZLH-SS-ISO nanocomposites.

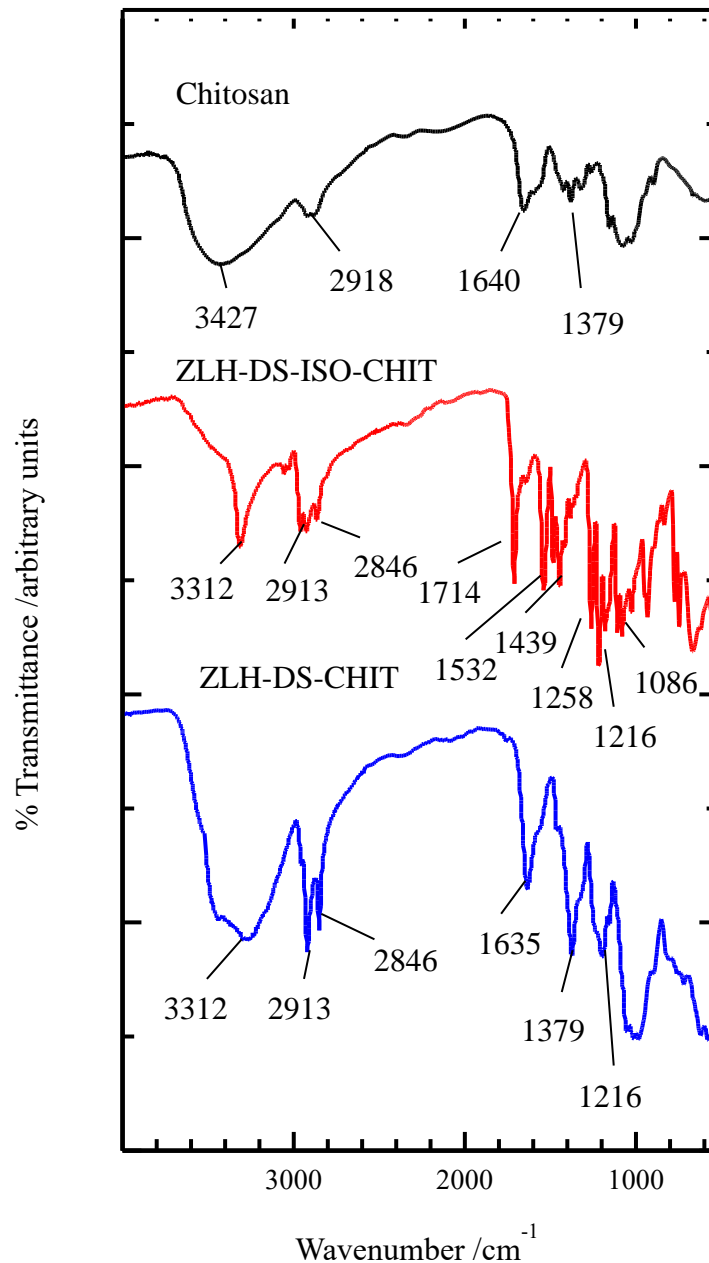


Figure 2 FTIR spectra of ZLH-DS-CHIT, ZLH-DS-ISO-CHIT nanocomposites and chitosan

Figure 3 shows the FTIR spectra that supported the successful coating process of CA onto the surface of ZLH-DS and ZLH-DS-ISO nanocomposites. A weak absorption peak for CA coated ZLH-DS at 3580 cm^{-1} and 1635 cm^{-1} was attributed to O-H vibration and H-O-H in the interlayer H_2O , respectively. On the other hand, the strong absorption peak at 3479 cm^{-1} was due to the hydroxyl group stretching vibrations of free water molecules. The peaks at 1736 cm^{-1} , 1216 cm^{-1} , and 1031 cm^{-1} were

superimposed from the CA spectra, due to the C-O, C-O (carboxylate), and C-O-C (pyranose ring) stretching vibrations. This absorption peak proved that ZLH-DS had been coated with CA. A few absorption peaks were overlaid on each other, such as the N-H and H-O-H peaks, the sulphate group with the C-O from a carboxylate group, and the stretching vibration of C-N with the aliphatic group stretching vibration (C-H, at 1368 cm^{-1}).

The FTIR spectra for the ZLH-DS-ISO-CA nanocomposite show absorption peaks that resemble both the CA molecule and the ZLH-DS-CA nanocomposite. The broad peak of the OH group at 3460 cm^{-1} in the CA coated nanocomposite was superimposed on CA's peak. Meanwhile, the sharp and intense peak at 1736 cm^{-1} , 1216 cm^{-1} , 1031 cm^{-1} , 1437 cm^{-1} , and 1368 cm^{-1} corresponded to the vibration of C-O, C-O (carboxylate), C-O-C (pyranose ring), and aliphatic group bending vibration, respectively. In the meantime, the peaks at 1368 cm^{-1} (C-N and C-H), 1216 cm^{-1} (S=O), and 1635 cm^{-1} (N-H) in ZLH-DS-ISO-CA were similar to the vibration peak in ZLH-DS-CA spectra.

The FTIR peak for CA was similar to the typical FTIR spectra in previously reported studies[56, 57]. The FTIR peak that corresponded to the OH group stretching vibrations for free water molecules was observed at 3460 cm^{-1} . The sp^3 stretching vibration of the C-H peak was detected at 2944 cm^{-1} and 2884 cm^{-1} . The other peaks at 1736 cm^{-1} , (1437 cm^{-1} and 1368 cm^{-1}), 1216 cm^{-1} , and 1031 cm^{-1} corresponded to C-O, C-H, C-O (carboxylate), and C-O-C (pyranose ring) respectively. The last two peaks below 1000 cm^{-1} existed in all three spectra. The vibration of the cyclic or acyclic aliphatic group was observed at 902 cm^{-1} . Subsequently, the vibration of O-H (out of plane) was observed at 602 cm^{-1} . All absorption peaks are listed in Table 2.

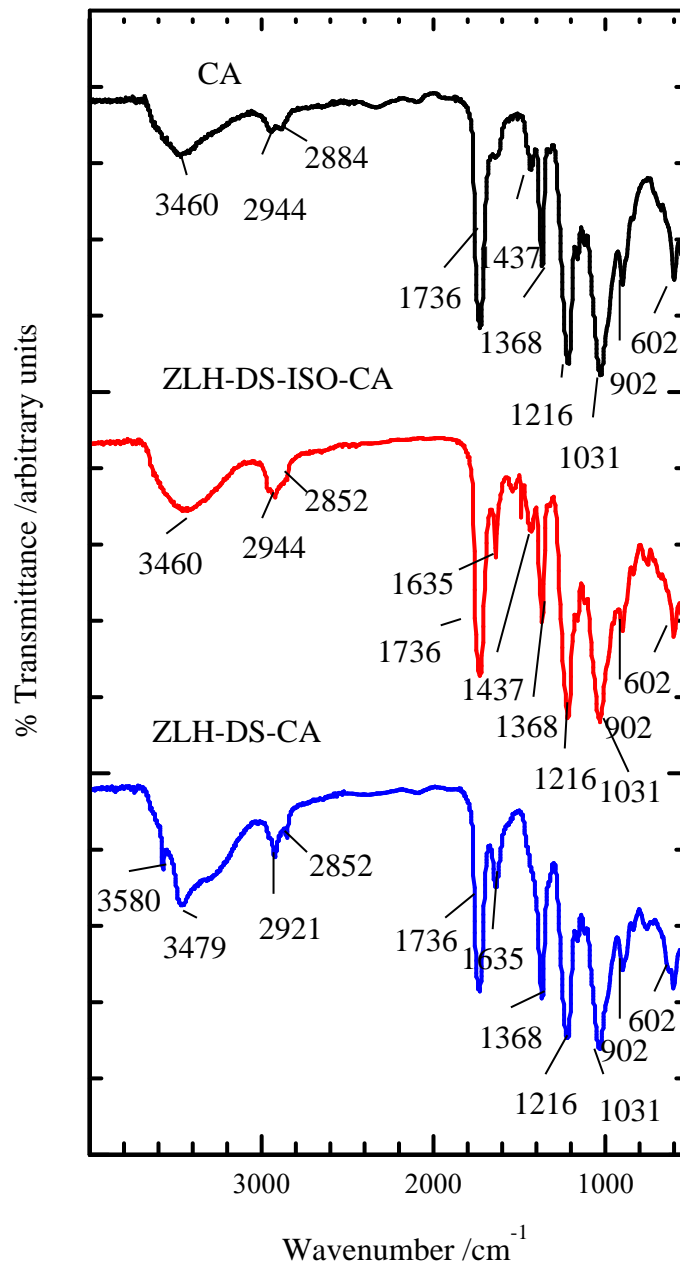


Figure 3 FTIR spectra for ZLH-DS-CA, ZLH-DS-ISO-CA nanocomposite and CA

Table 1

FTIR peaks for ZLH-DS-CHIT, ZLH-DS-ISO-CHIT nanocomposites and Chitosan

Characteristic group	ZLH-DS-CHIT (cm-1)	ZLH-DS-ISO-CHIT (cm-1)	Chitosan (cm-1)
v (O-H), H-bonded	3312	3312	3427
v (O-H) in the interlayer; H ₂ O	-	-	-
v (H-O-H) in the interlayer; H ₂ O	1635	-	-
v (C-N)	1379	1258	1379
v (C-H), stretching	2846 2913	2846 2913	2918
v (C-H), bending	-	1532 1439	-

v (N-H), stretching	-	-	3427
v (N-H),bending	1635	1714	1640
v (N-O)	1379	-	-
vas (S=O)	1216	1216	-
vs (S=O)	-	1086	-

Table 2

FTIR peaks for ZLH-DS-CA, ZLH-DS-ISO-CA nanocomposites and CA

Characteristic group	ZLH-DS-CA (cm-1)	ZLH-DS-ISO-CA (cm-1)	Cellulose acetate (cm-1)
v (O-H), H-bonded	3479	3460	3460
v (O-H) in the interlayer; H ₂ O	3580	-	-
v (H-O-H) in the interlayer; H ₂ O	1635	1635	-
v (C-O)	1736	1736	1736
v (C-O), carboxylate	1216	1216	1216
v (C-O-C), pnyranose ring	1031	1031	1031
v (C-N)	1368	1368	-
v (C-H),stretching	2852 2921	2852 2944	2884 2944
v (C-H),bending	1368	1437 1368	1437 1368
v (N-H), stretching	-	-	-
v (N-H),bending	1635	1635	-
vas (S=O)	1216	1216	-
vs (S=O)	-	1031	-
vas (ring) or v (C-H),out of plane	902	902	902
γ OH (out of plane)	602	602	602

3.3 Thermal study

Thermal studies of chitosan-coated nanocomposites (ZLH-DS-CHIT and ZLH-DS-ISO-CHIT) were determined using TGA-DTG analyses (Figure 4). Figure 4 (a) depicts two stages that occurred at T_{max} of 96 °C and 367 °C, with weight loss of 5.9% and 64.0%, respectively. This stage was attributed to losses of moisture while the other stage of weight loss referred to the decomposition of deacetylated chitosan units and the dehydration of saccharide rings[58].

The thermal decomposition of coated ZLH-DS has four weight-loss stages, as shown in Figure 4 (b). At a T_{max} of 79 °C, the 9.6% weight loss (first stage) corresponds to moisture loss. The partial decomposition of the SDS and dehydroxylation of the layers²⁹ were referred to in the second stage at T_{max} of 167 °C with 4.9 % weight loss. The SDS was decomposing at T_{max} of 246 °C with a weight loss of 49.0% (third stage). The last weight loss stage was attributed to the decomposition of an amorphous mixture of salts that was generated during the initial SDS decomposition at T_{max} of 887 °C with 13.4% weight loss[59]. By comparing the total weight loss of coated ZLH-DS (76.9 %) with uncoated ZLH-DS (40.2%), it could be concluded that ZLH-DS had been coated by 36.7% of chitosan.

Figure 4(c) depicts two stages of weight loss during the thermal decomposition of a ZLH-DS-ISO-CHIT nanocomposite. The first stage of weight loss at T_{max} of 170 °C by 53.3 % was due to the decomposition of isoproc carb anion, while the second stage of weight loss (43.2%) at T_{max} of 263 °C was due to the decomposition of SDS. Both thermal decompositions had a slight shift from the uncoated nanocomposite. However, the temperatures were still in the same ranges, which were 135 °C-200 °C and 200 °C-270 °C for the decomposition of isoproc carb anion and SDS respectively. The thermal stability of coated ZLH-DS-ISO slightly decreased compared to uncoated nanocomposite. This resulted from the nanocomposite molecule precipitating outside

the chitosan matrix, as previously reported by Li et al.⁶⁰. The total weight loss of coated ZLH-DS-ISO was 96.5% which was higher than the total weight loss of uncoated nanocomposite (93.0%). Based on the percentage difference between uncoated and coated nanocomposite, ZLH-DS-ISO nanocomposite was successfully coated with 3.5% chitosan [28, 39, 53].

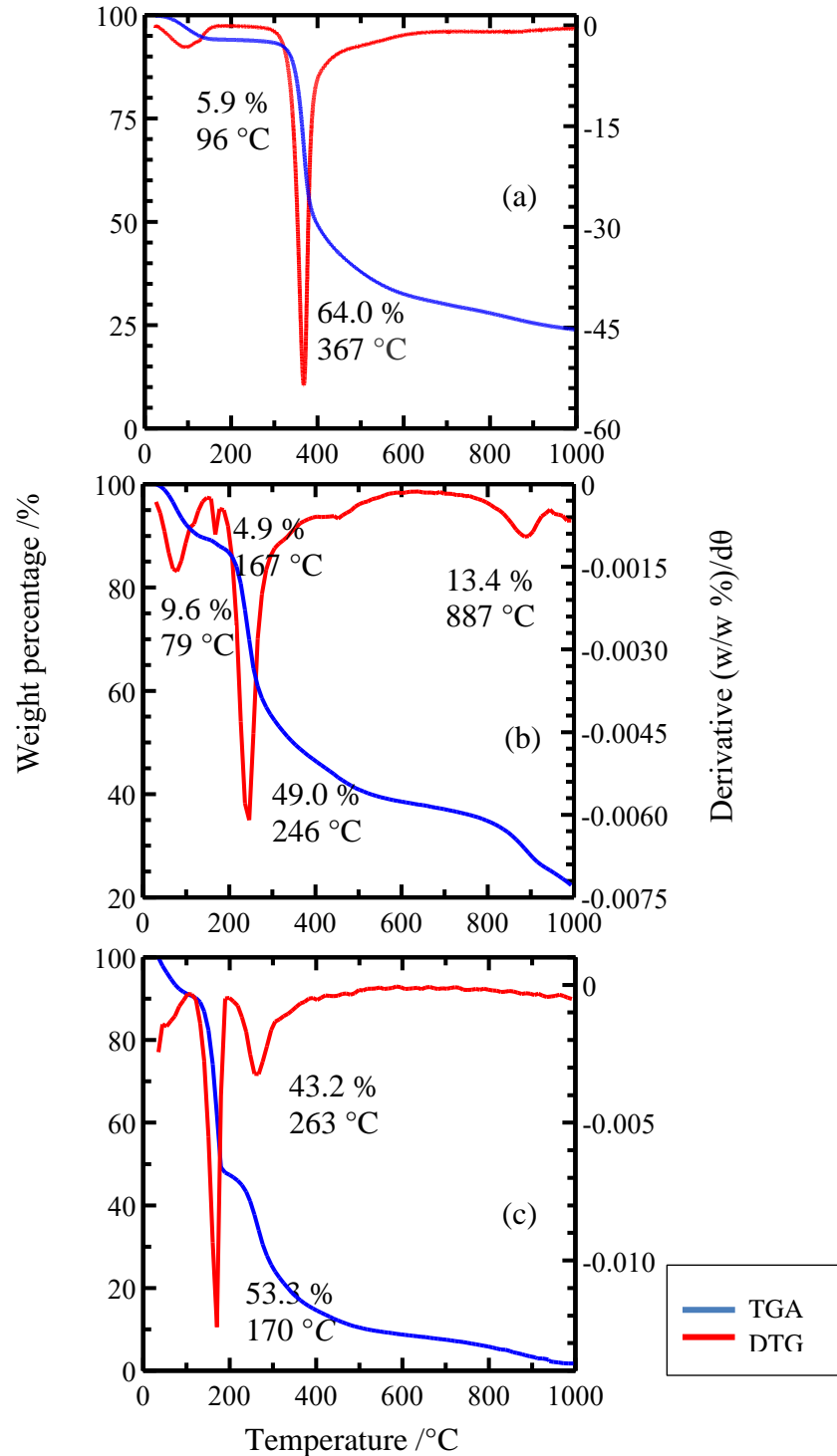


Figure 4 TGA/DTG curve for (a) chitosan, (b) ZLH-DS-CHIT, and (c) ZLH-DS-ISO-CHIT nanocomposite

Figure 5 displays the thermal behaviour of ZLH-DS-CA and ZLH-DS-ISO-CA nanocomposites after coating by CA. At T_{max} of 355 °C (weight loss of 84.6%), a single thermal event was clearly observed in cellulose acetate, which is due to the decomposition of the cellulose acetate matrix, which caused the formation of volatile gaseous then leaving a stable carbonaceous residue[60].

Figure 5(b) shows two steps of thermal decomposition for coated ZLH-DS. The first step of weight loss (6.4%) at T_{max} of 99 °C corresponded to moisture loss. The next steps of weight loss at T_{max} of 340 °C with a values of 66.4% corresponded to the dehydroxylation of the layers and the decomposition of SDS. By subtracting the total weight loss of ZLH-DS-CA (72.8%) from the uncoated ZLH-DS (40.2%), it could be suggested that 32.6 % of CA had coated the ZLH-DS.

Meanwhile, Figure 5(c) depicts the thermal decomposition of the ZLH-DS-ISO-CA nanocomposite, distinguished by two weight loss stages. The first stage of decomposition occurred at T_{max} of 153 °C and resulted in a 15.8% weight loss, followed by a second weight loss (78.4%) at T_{max} of 353 °C. Similar to the thermal decomposition of ZLH-DS-ISO-CHIT, the first stage corresponded to the decomposition of isoprocarb while the second stage corresponded to the decomposition of SDS.

Based on the above discussion, it can be suggested that the ZLH-DS-ISO-CA nanocomposite has low thermal stability compared to the ZLH-DS-ISO-CHIT nanocomposite. The CA itself degrades at a low temperature compared to pure chitosan, thus decreasing the degradation temperature of isoprocarb anion. The total weight loss for coated ZLH-DS-ISO is 94.2%, which is relatively higher than the total weight loss of uncoated nanocomposite (93.0%). It can therefore be assumed that the nanocomposite ZLH-DS-ISO was covered with 1.2% CA[12, 44].

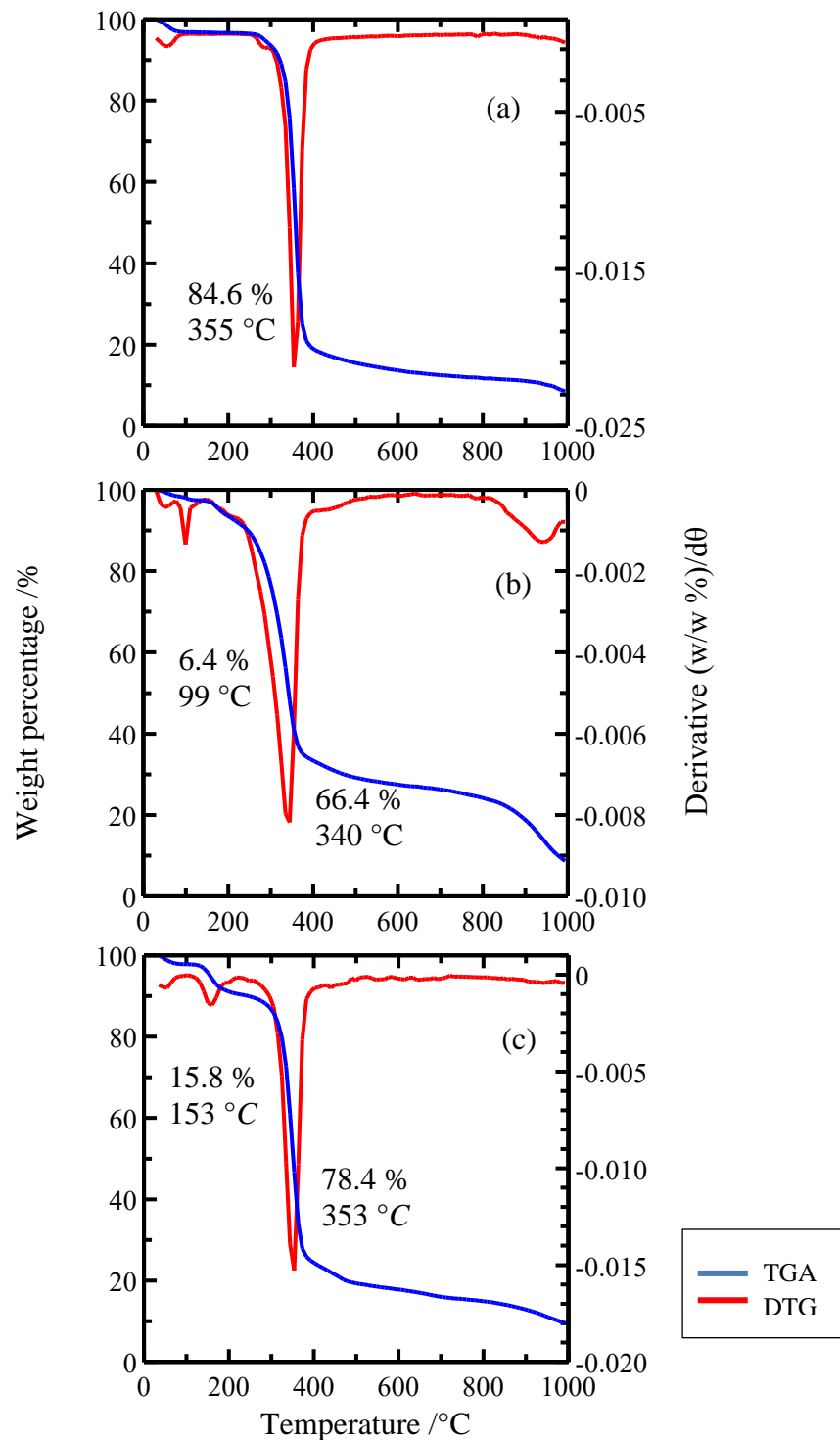


Figure 5 TGA/DTG curve for (a) CA, (b) ZLH-DS-CA, and (c) ZLH-DS-ISO-CA nanocomposites

3.4 Surface morphology

The surface morphology for chitosan, ZLH-DS-CHIT and the ZLH-DS-ISO-CHIT nanocomposites was observed by FESEM (Figure 6). Chitosan showed a typical surface characteristic with a compact and smooth surface[61, 62]. The coated ZLH-DS shows a structure of sea sponge-like agglomeration with rough surface morphology compared to pristine chitosan. Whereas, the coated nanocomposite demonstrated a compact, simple, dense, and contiguous structure, similarly as

reported by other studies[63]. When compared to pure chitosan, the surfaces of ZLH-DS-ISO-CHIT nanocomposite had no interface layer and were more homogeneous. The formation of a homogeneous surface is probably caused by the interactions of the functional groups and hydrogen bonds that exist on coated nanocomposite[44].

The surface morphology of pure CA and ZLH-DS-ISO-CA nanocomposite bulk fractures is shown in Figure 7. The pure cellulose acetate surface revealed a smooth fracture which corresponded to a dense polymer film[64]. The surface morphology of the CA-coated ZLH-DS was similar to that of the chitosan-coated ZLH-DS. Its surface was rougher than the pure cellulose acetate, indicating successful encapsulation of ZLH-DS into cellulose acetate[46]. Meanwhile, the surface of the ZLH-DS-ISO-CA was rough, which could structurally increase the surface area of the ZLH-DS-ISO-CA, as previously described. Once ZLH-DS-ISO-CA was put into the water, it could absorb water and form a swollen hydrogel. This finding is consistent with the previously reported water-retention property for controlled release formulations of ZLH-DS-ISO-CA nanocomposites[65, 66].

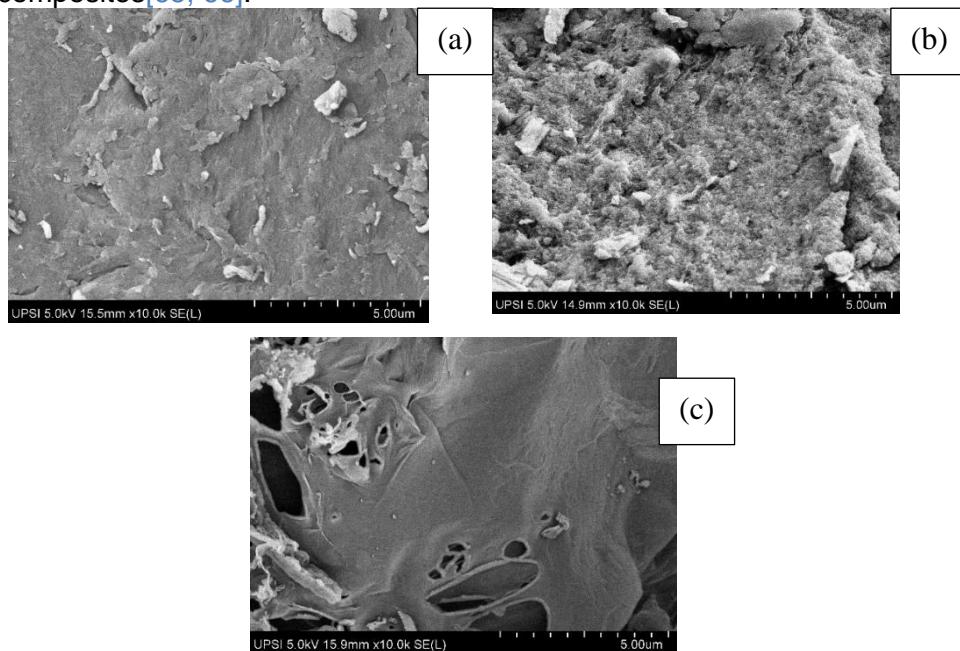


Figure 6 FESEM images (10K magnification) of (a) chitosan, (b) ZLH-DS-CHIT, and (c) ZLH-DS-ISO-CHIT nanocomposites

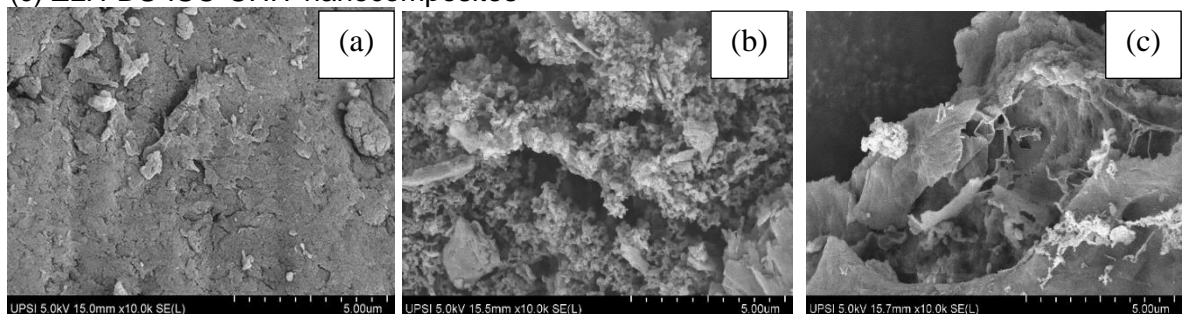


Figure 7 FESEM images (10K magnification) of (a) CA, (b) ZLH-DS-CA, and (c) ZLH-DS-ISO-CA nanocomposites

3.5 The release study of isoprocab anion from chitosan and CA coated ZLH-DS-ISO nanocomposite

Figure 8 (a), (b), and (c) indicate the release profiles of ISO anion from the interlayer of the ZLH-DS-ISO-CHIT nanocomposites into 0.1 M, 0.2 M, and 0.3 M of Na₃PO₄, Na₂SO₄, and NaCl solutions, respectively. The figure shows that, the

accumulated release of isoproc carb anion increased with contact time for all concentrations of release solutions. The release rate in all solutions was fast-moving at the first 1000 min, followed by a slow-moving until 1500 min, before it reached equilibrium at 2000 min.

The isoproc carb anion release profiles from the interlayer of ZLH-DS-ISO-CA nanocomposites into various concentrations of Na_3PO_4 , Na_2SO_4 , and NaCl solutions (0.1 M, 0.2 M, and 0.3 M) are shown in Figure 9 (a), (b), and (c), respectively. The release of ISO anion into Na_3PO_4 and Na_2SO_4 solutions displayed a similar pattern. ISO anion was released abruptly for the first 500 min, then slowly until it reached equilibrium at 1500 min. Meanwhile, the release of the ISO anion from the interlayer of ZLH-DS-ISO-CA into NaCl solution was rapid for the first 500 min, then moderate until it reached equilibrium at 2000 min.

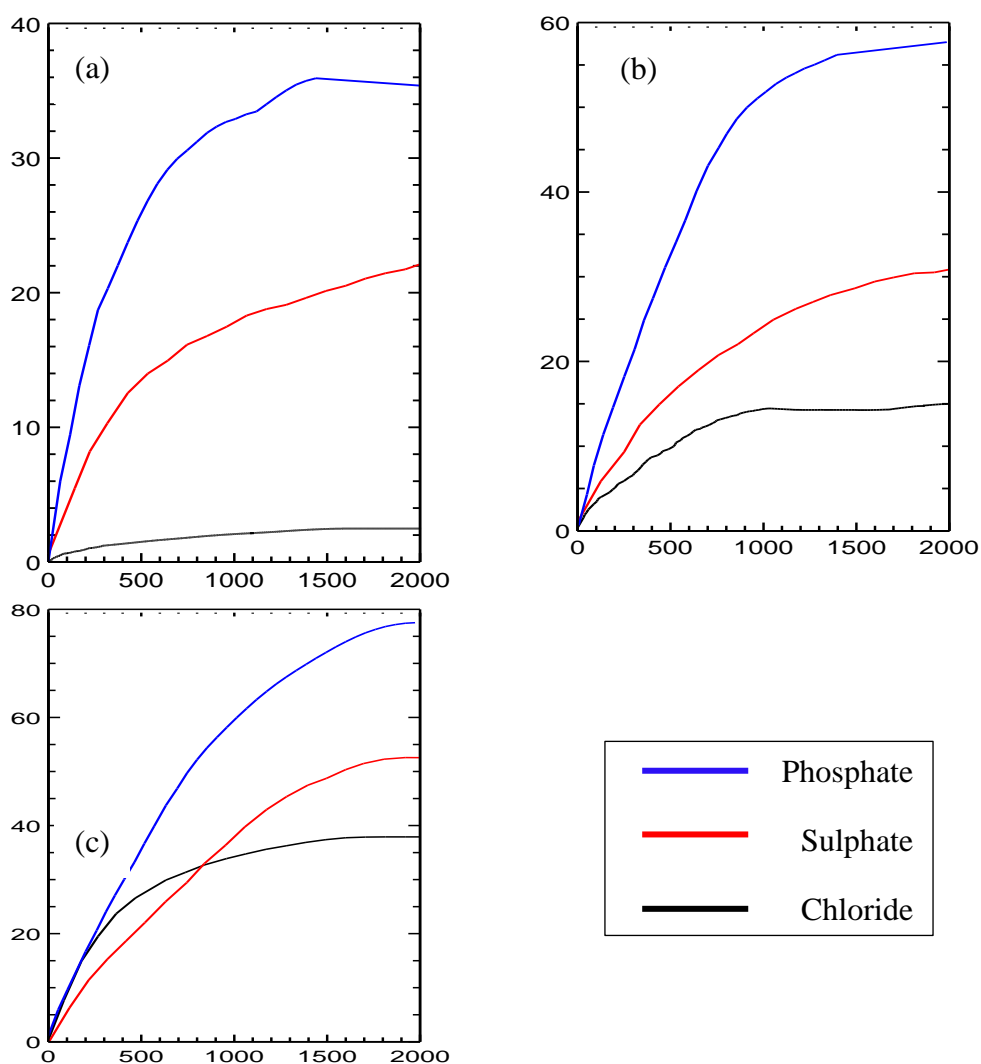


Figure 8 Release profile of ISO anion from ZLH-DS-ISO-CHIT nanocomposite into (a) 0.1 M, (b) 0.2 M and (c) 0.3 M concentration of aqueous Na_3PO_4 , Na_2SO_4 , and NaCl solutions

Figure 8 shows that the initial release of ISO anion from the interlayer of nanocomposites into all three solutions was rapid and then slowed until equilibrium was reached. The high density of incoming anion leads to the rapid release, whereas, the strong ISO interaction leads to the slower release[67]. [68] have reported that the release process depends on the existence of sacrificial anions in solutions. Sacrificial anions acted as a stimulus force to increase the release process of ISO anions into the solutions. Meanwhile, the low release rate of the anion in the matrix was due to the availability of free void spaces through which a lesser number of insecticide molecules could be transported. Furthermore, the ion exchange process occurred when a high-affinity sacrificial anion (phosphate, sulphate, and chloride anions) was applied to the ZLH compared to the ISO existing counter anion[69]. Additionally, the presence of chitosan and CA as coaters for ZLH-DS-ISO nanocomposite will create an initial burst of open release followed by a gradual release of isoprocarb. The initial burst open release involved isoprocarb diffusion as a result of rapid swelling and was partially related to adsorbed on the nanocomposite surface.

As shown in Figure 8, the accumulated release of ISO anion from ZLH-DS-ISO-CHIT into Na_3PO_4 solution was dominated by 36.0 %, 56.4 %, and 77.6 % of release percentage for 0.1 M, 0.2 M, and 0.3 M, respectively, compared to Na_2SO_4 and NaCl solutions. In Na_2SO_4 solution, the percentage of accumulated release was 25.0%, 30.8%, and 52.6% in 0.1 M, 0.2 M, and 0.3 M, respectively, whereas in NaCl solution, the percentage was 2.4%, 15.0%, and 37.8% in 0.1 M, 0.2 M, and 0.3 M, respectively.

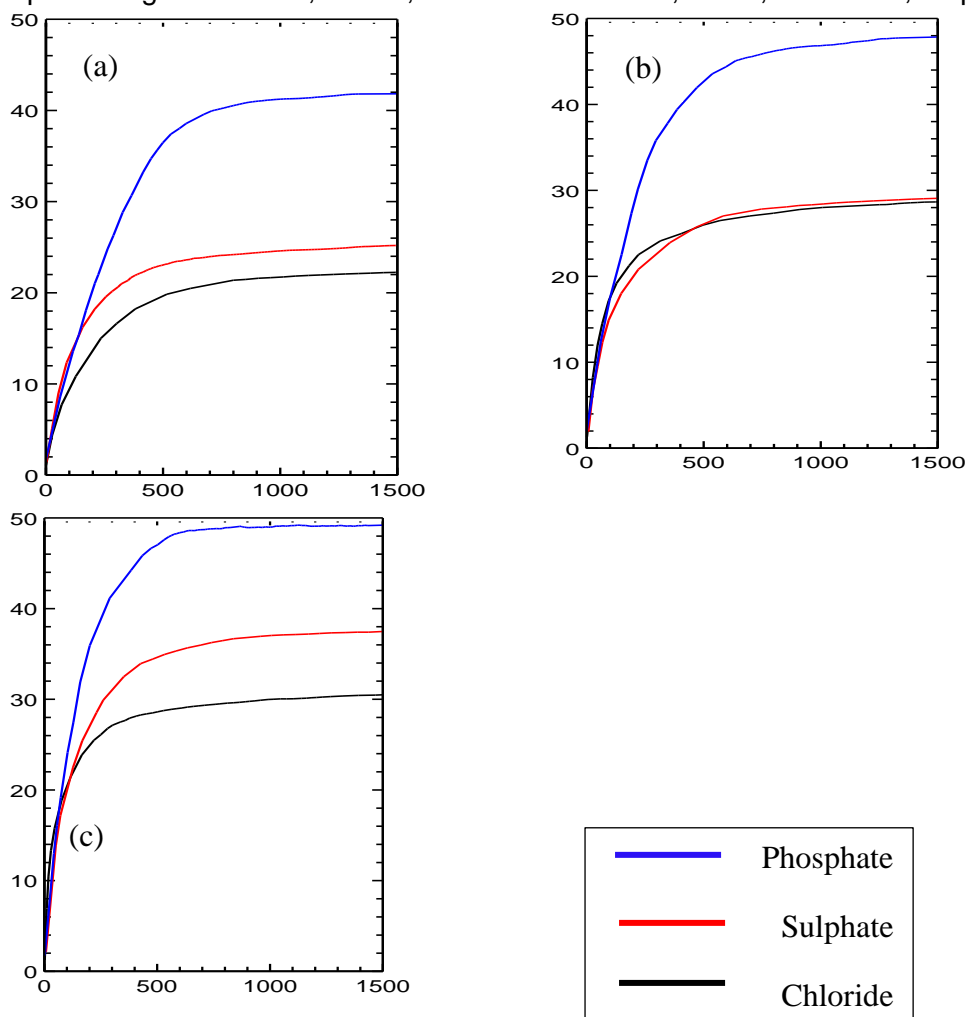


Figure 9 Release profile of ISO anion from ZLH-DS-ISO-CHIT nanocomposite into (a) 0.1 M, (b) 0.2 M and (c) 0.3 M concentration of aqueous Na_3PO_4 , Na_2SO_4 , and NaCl solutions

The release profile of the ISO anion from ZLH-DS-ISO-CA was found to be higher in Na₃PO₄ solution with an accumulated percentage release of 38.8% (0.1 M), 47.8% (0.2 M), and 49.1% (0.3 M). The accumulated release of ISO anion into Na₂SO₄ solution is lower than Na₃PO₄ solution but higher than NaCl solution, with values of 22.5% (0.1 M), 29.2% (0.2 M), and 37.8% (0.3 M). In the NaCl solution, the percentage release was 20.5% (0.1 M), 28.7% (0.2 M), and 30.7% (0.3 M). As previously discussed, phosphate ion with three charges has the highest affinity, resulting in strong electrostatic attraction towards ZLH, followed by sulphate (two charges) and chloride ion (one charge)[69-71]. For this reason, the percentage release of ISO anion was higher in Na₃PO₄ solutions than in Na₂SO₄ and NaCl solutions. Table 3 shows the accumulated percentage release of ISO anion from ZLH-DS-ISO-CHIT and ZLH-DS-ISO-CA nanocomposites.

Table 3

Percentage of ISO anion release from ZLH-DS-ISO-CHIT and ZLH-DS-ISO-CA nanocomposites into various solutions

Concentration (M)	Na ₃ PO ₄ solution (%)		Na ₂ SO ₄ solution (%)		NaCl solution (%)	
	ZLH-DS-ISO-CHIT	ZLH-DS-ISO-CA	ZLH-DS-ISO-CHIT	ZLH-DS-ISO-CA	ZLH-DS-ISO-CHIT	ZLH-DS-ISO-CA
0.1	36.0	38.8	25.0	22.5	2.4	20.5
0.2	56.4	47.8	30.8	29.2	15.0	28.7
0.3	77.6	49.1	52.6	37.8	37.8	30.7

The results demonstrate that the percentage release in coated nanocomposites was lower than in uncoated nanocomposites, which is consistent with Ghamami et al.'s⁴⁷ findings. This phenomenon was due to an increased degree of protection of the chitosan and CA-coated nanocomposite.

The accumulated percentage of ISO anion from ZLH-DS-ISO-CHIT shows a slower release compared to uncoated ZLH-DS-ISO and ZLH-DS-ISO-CA nanocomposites. Such an observation could be related to the orientation and arrangement of the anion within the intergallery matrix. From the PXRD analysis of ZLH-DS-ISO nanocomposite²⁷, the anion was arranged in a well-ordered manner with high crystallinity compared to ZLH-DS-ISO-CHIT and ZLH-DS-ISO-CA nanocomposites. Therefore, the release of ISO anion from the interlayer ZLH-DS-ISO should be slower compared to coated nanomaterial [71, 72]. This study shows that the release of ISO anion from coated nanocomposite (low crystallinity) is slower than uncoated nanocomposite (high crystallinity). This observation was due to the increase of the hydrogen bond and electrostatic attraction among the host, chitosan/CA, and ISO anion, as in a similar study done by [73]. According to the findings, chitosan is an effective coating for ZLH-DS-ISO nanocomposites that can continuously release isopropyl carbon anions

3.6 Kinetic study of ISO anion from chitosan and CA coated ZLH-DS-ISO nanocomposites

The release behaviour of ISO anion between the interlayers of coated ZLH-DS-ISO nanocomposites was studied using five kinetic models, namely, Zeroth order (eq. 1)[74], First order (eq. 2)[75], Pseudo-second order (eq. 3)[76], Parabolic Diffusion model (eq. 4)[77] and the Fickian Diffusion model (eq. 5)[78]. The following are the model equations.

$$x = t + C$$

$$-\log (1- M_i/M_f) = t + C$$

$$t/ M_i = 1/ M_f^2 + t / M_f$$

$$M_i / M_f = kt^{1/2} + C$$

$$M_i/M_f = kt^n$$

x = percentage of isoproc carb anion release over time t , M_i = initial concentration, M_f = final concentration, C = constant, n = an empirical parameter and rate constant k . $t_{1/2}$ = time required for nanocomposite to release 50% of ISO anion

The obtained fitting curve for ZLH-DS-ISO-CHIT nanocomposite (0 to 500 min) is presented in Figures 10 to 12. The first order was followed by the ISO anion release into the Na_3PO_4 solution. Whereas the ISO anion release into Na_2SO_4 and NaCl solutions followed the parabolic diffusion model. The fitting data obtained (k , $t_{1/2}$, and r^2) are listed in Table 4. Meanwhile, the cumulative releases of the ISO anion from ZLH-DS-ISO-CA nanocomposite were fitted to the kinetic models shown in Figures 13 to 15. The data was plotted between 0 and 500 min, which shows that the release of ISO anion into all three solutions followed the pseudo-second-order. The calculated values of k , $t_{1/2}$, and r^2 are listed in Table 5.

As shown in Table 4 (release profile for ZLH-DS-ISO-CHIT nanocomposite), the rate constant (k) and $t_{1/2}$ increased with increasing concentration of sodium phosphate solution which indicated that, the release of ISO anion depended on the concentration of incoming anion. This is consistent with the first-order kinetic model that demonstrated the release process, in which the dissolution rate was determined solely by the concentration of one reactant[23]. The parabolic diffusion kinetic model, on the other hand, emphasises the diffusion-controlled system, which is controlled by surface diffusion or intraparticle diffusion[79]. [32, 44] reported that the surface diffusion or intra particle diffusion via ion exchange process was the rate-determining step in the release mechanism. Table 4 shows the release rate and $t_{1/2}$ for ISO anion releases into Na_2SO_4 and NaCl solutions, which showed a nearly identical pattern. The release rate and $t_{1/2}$ for both solutions increased with the increasing sulphate and chloride concentrations, due to the strong electrostatic interaction between ZLH and ISO anion that affected the diffusion rate in Na_2SO_4 and NaCl solutions.

The release rate of the ZLH-DS-ISO-CA nanocomposite increased with the increasing concentration of release solution while the $t_{1/2}$ decreased. This was due to the fact that at higher concentrations of the release solution, more ISO anion could be released, resulting in a rapid ion exchange process between the ISO anion and the incoming anion. The $t_{1/2}$ values for ISO anion release between the interlayers of ZLH-DS-ISO-CA nanocomposite into NaCl solutions were higher compared to Na_3PO_4 and Na_2SO_4 solutions, which indicated that the release of ISO anion in NaCl solution was slower compared to the other two solutions[80]. This was attributable to chloride ions' lower affinity, which resulted in a slower rate of ISO release from its nanocomposite[81].

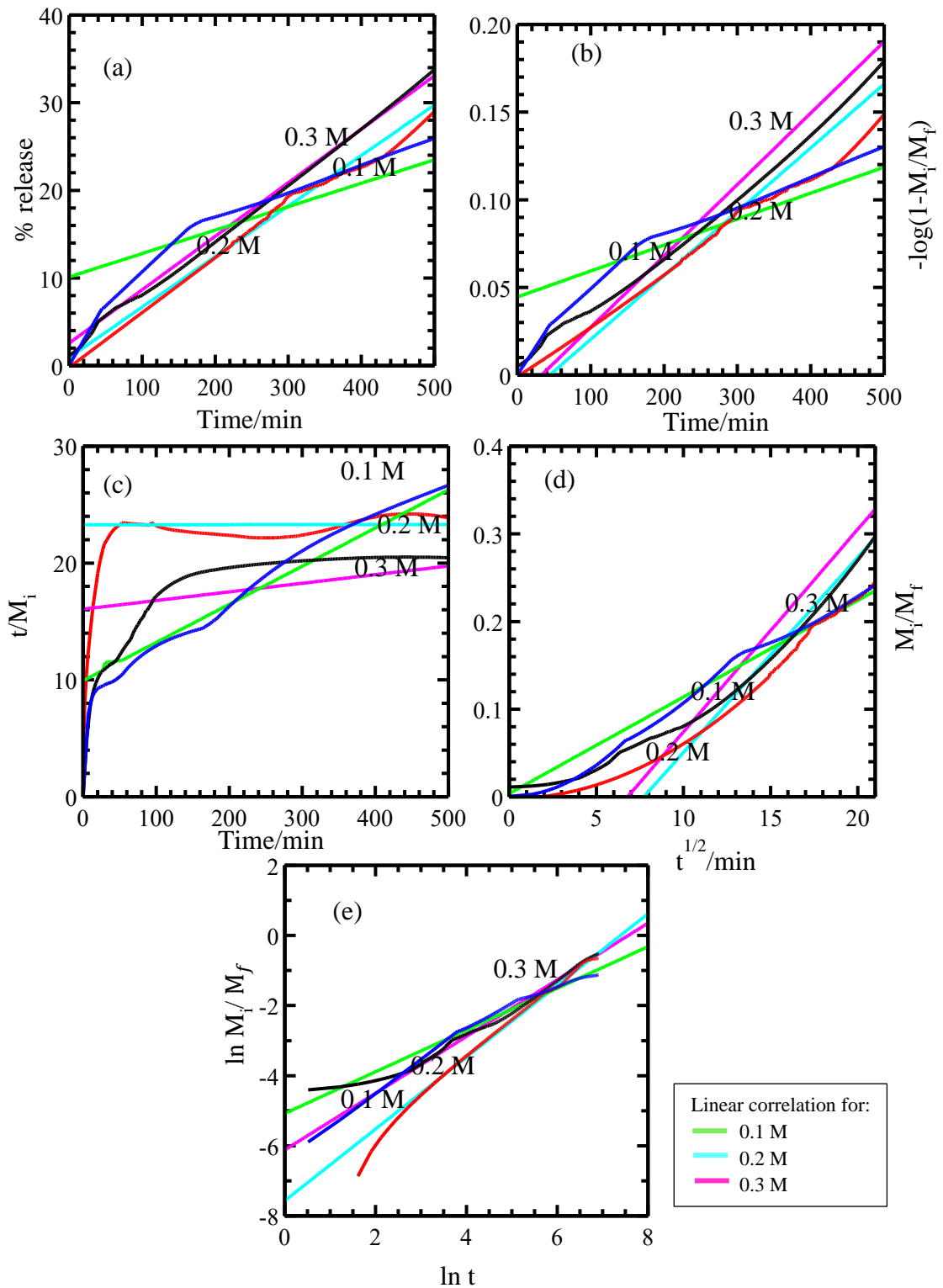


Figure 10 Kinetic fitting data for ZLH-DS-ISO-CHIT nanocomposite in various concentration of Na_3PO_4 solutions: (a) zeroth, (b) first, (c) pseudo-second-order, (d) parabolic diffusion, and (e) Fickian diffusion

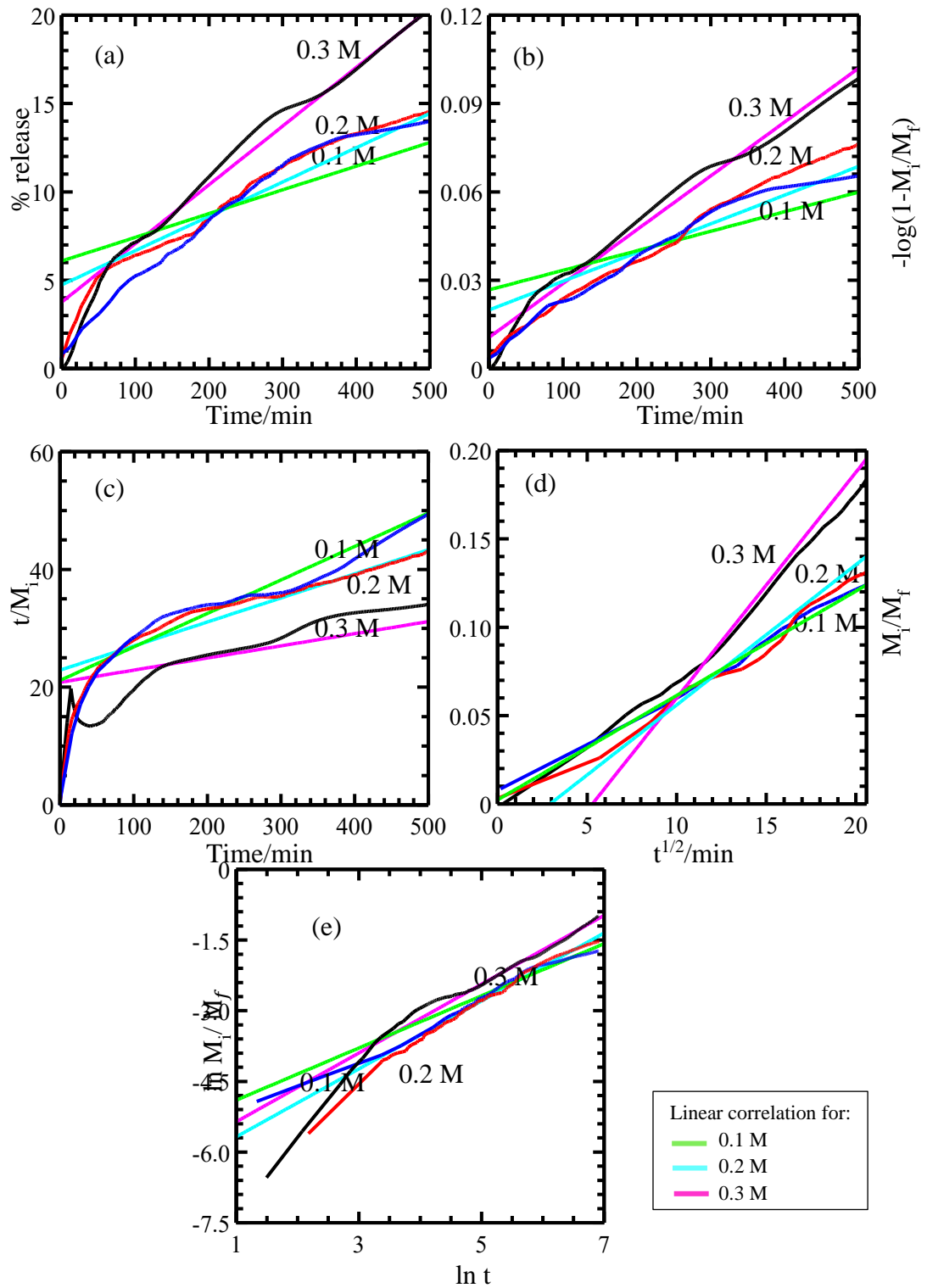


Figure 11 Kinetic fitting data for ZLH-DS-ISO-CHIT nanocomposite in various concentration of Na_2SO_4 solutions: (a) zeroth, (b) first, (c) pseudo-second-order, (d) parabolic diffusion, and (e) Fickian diffusion

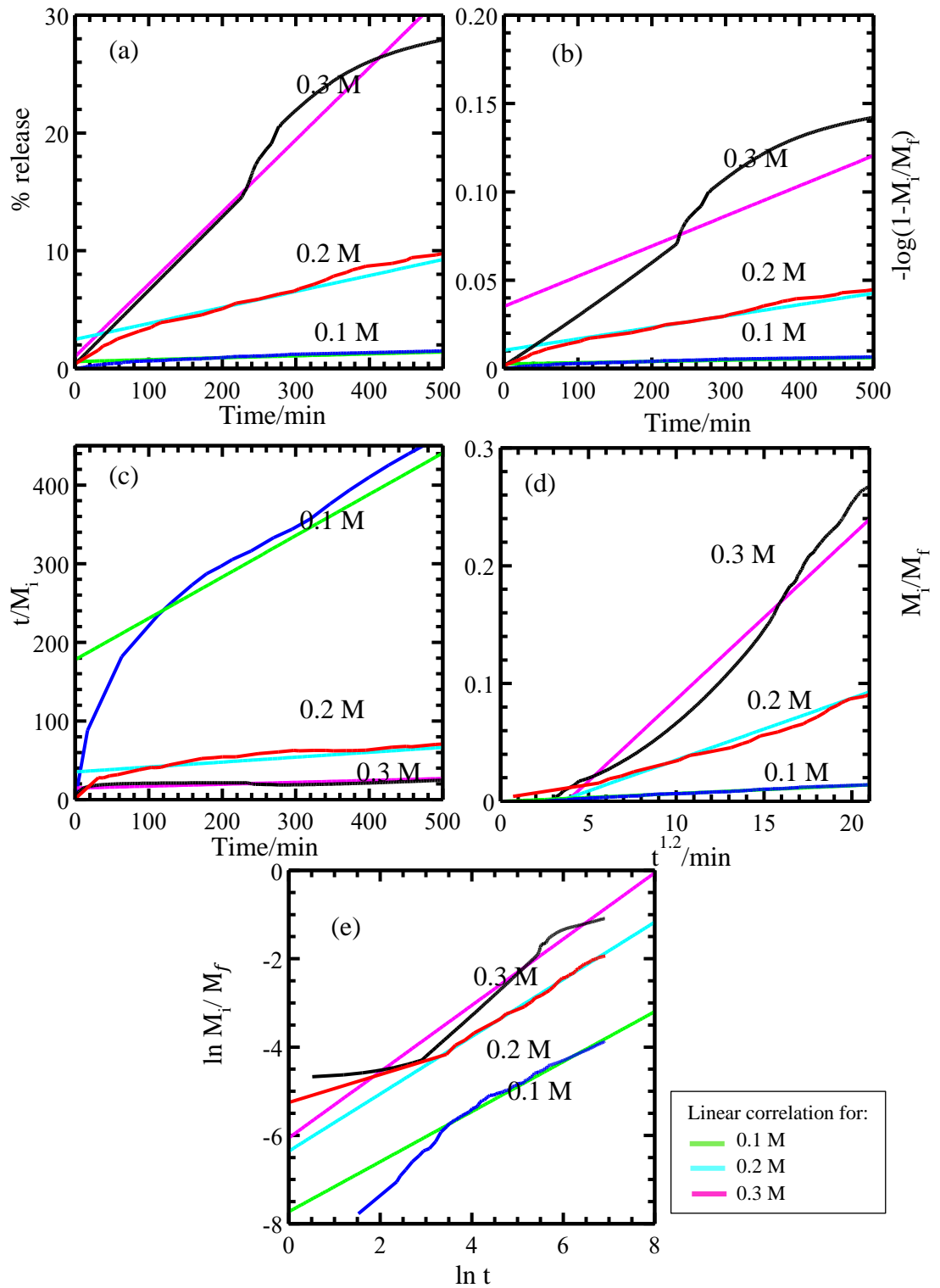


Figure 12 Kinetic fitting data for ZLH-DS-ISO-CHIT nanocomposite in various concentration of NaCl solutions: (a) zeroth, (b) first, (c) pseudo-second-order, (d) parabolic diffusion, and (e) Fickian diffusion

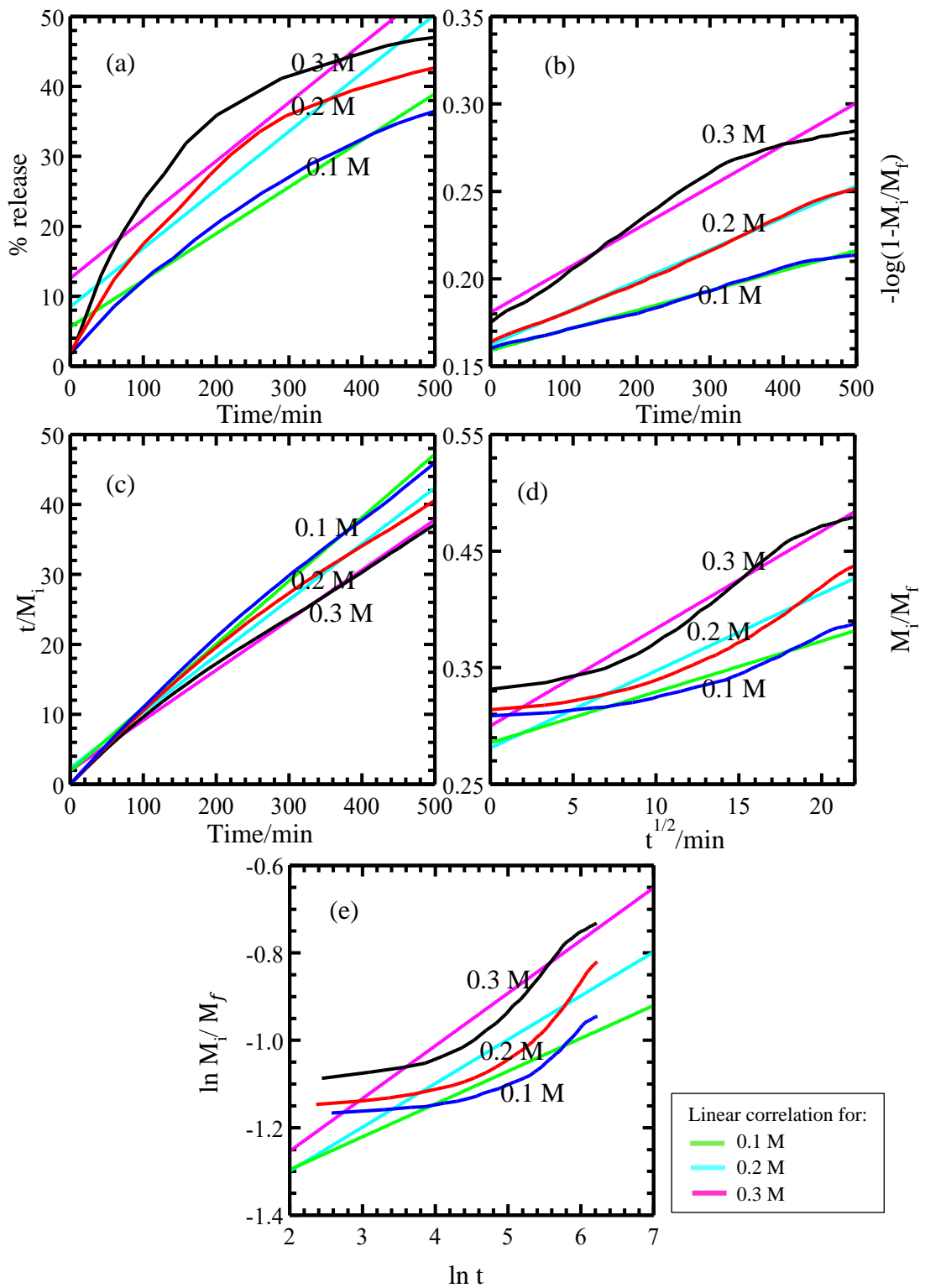


Figure 13 Kinetic fitting data for ZLH-DS-ISO-CA nanocomposite in various concentration of Na_3PO_4 solutions: (a) zeroth, (b) first, (c) pseudo-second-order, (d) parabolic diffusion, and (e) Fickian diffusion

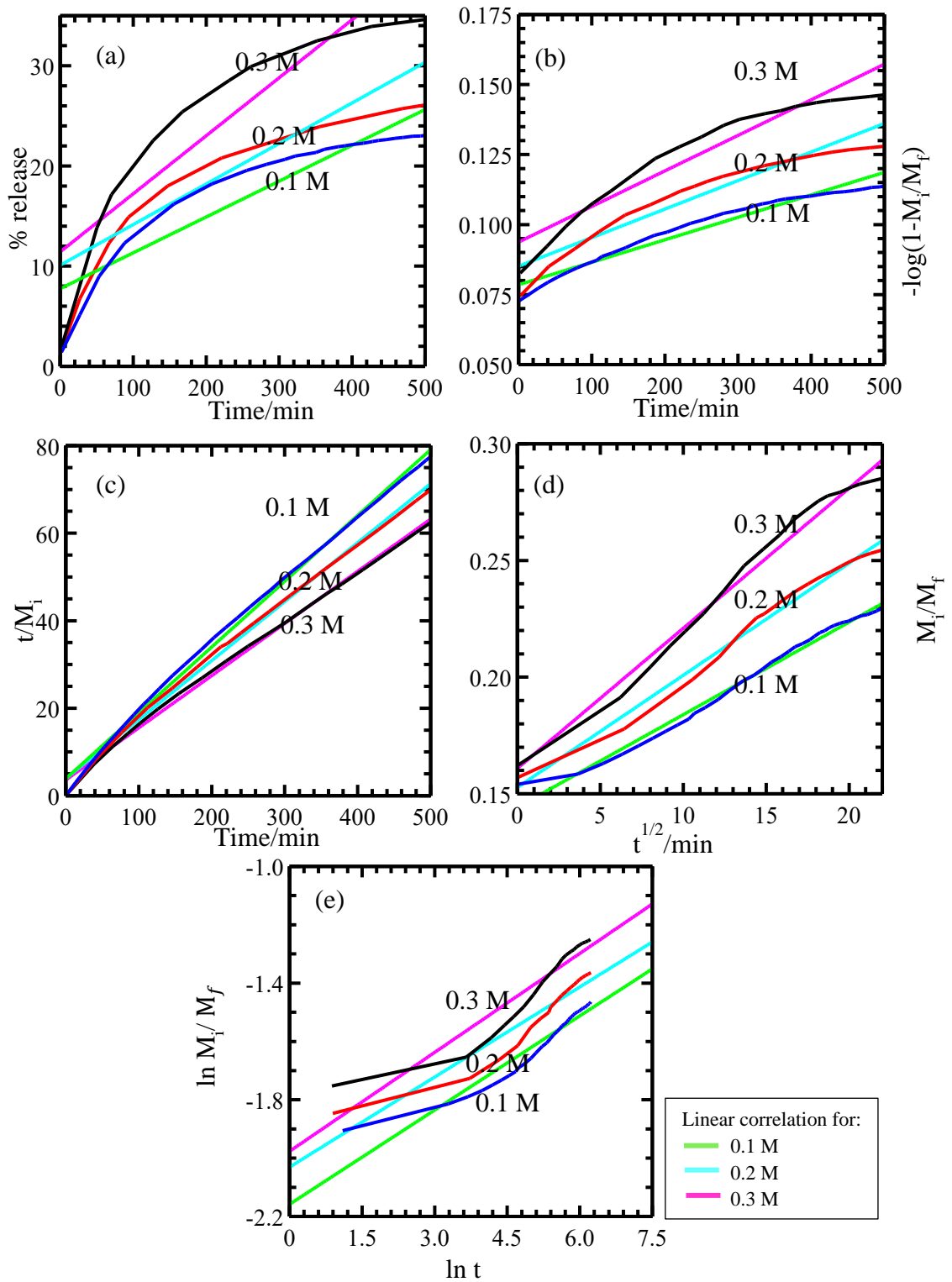


Figure 14 Kinetic fitting for ZLH-DS-ISO-CA nanocomposite in various concentration of Na_2SO_4 solutions: (a) zeroth, (b) first, (c) pseudo-second-order, (d) parabolic diffusion, and (e) Fickian diffusion

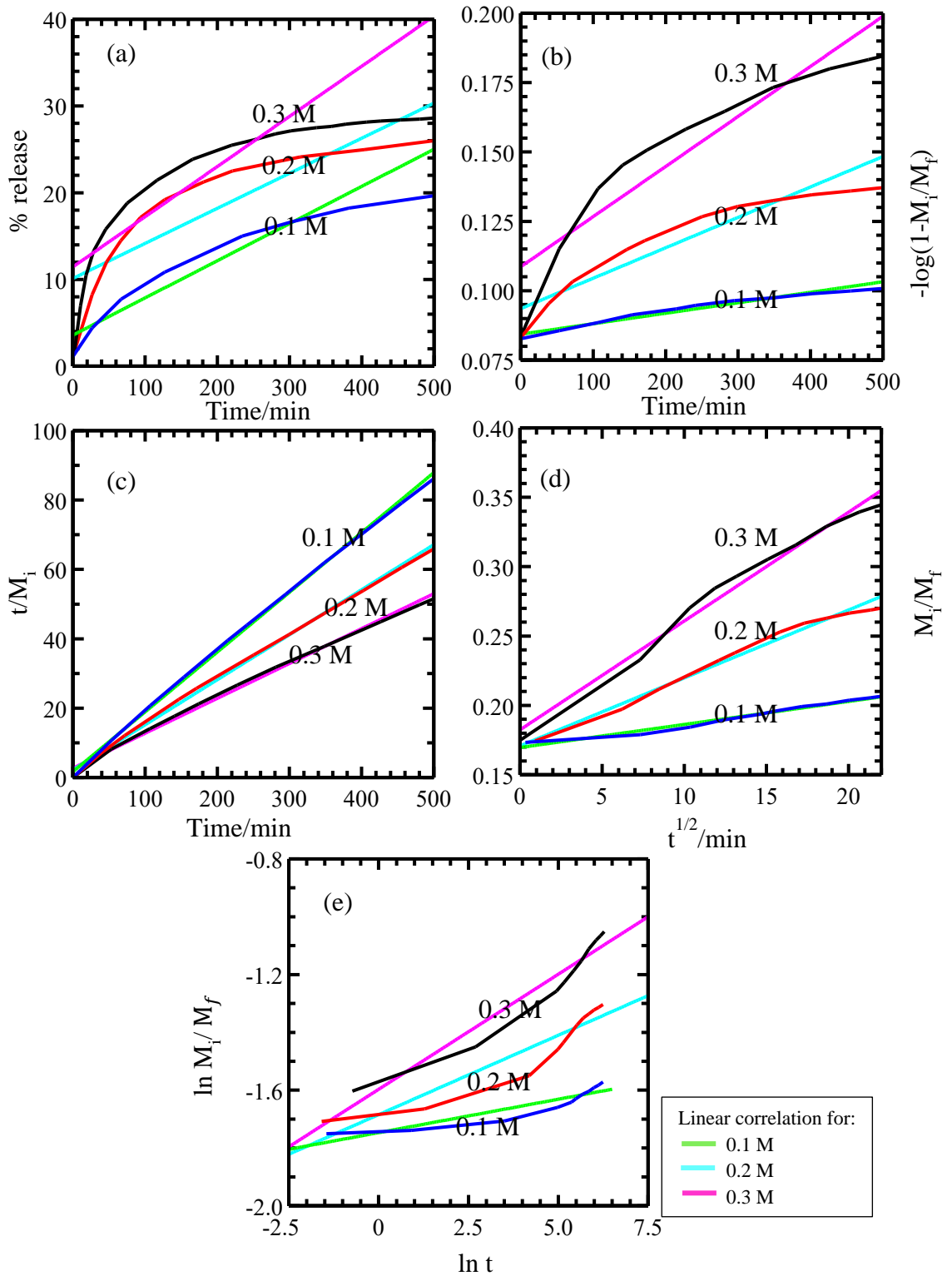


Figure 15 Kinetic fitting data for ZLH-DS-ISO-CA nanocomposite in various concentration of NaCl solutions: (a) zeroth, (b) first, (c) pseudo-second-order, (d) parabolic diffusion, and (e) Fickian diffusion

Table 4
Correlation coefficients (r^2), rate constant (k) and half-life ($t_{1/2}$) of isoprocab release from ZLH-DS-ISO-CHIT nanocomposite into solutions (Na_3PO_4 , Na_2SO_4 , NaCl)

Na ₃ PO ₄ (M)	Zeroth order	Pseudo-second-order	Parabolic diffusion	Fickian	First-order			
					r^2	k ($\times 10^{-4}$) (mol-1L s-1)	$t_{1/2}$ (min)	c ($\times 10^{-2}$)
0.1	0.894	0.992	0.984	0.957	0.922	1.48	202.6	4.45
0.2	0.984	0.003	0.959	0.994	0.983	3.64	512.6	1.61
0.3	0.994	0.512	0.965	0.984	0.994	4.07	533.8	1.35
Na ₂ SO ₄ (M)	Zeroth order	First-order	Pseudo-second-order	Fickian	Parabolic diffusion			
					r^2	k ($\times 10^{-3}$) (mol-1L s-1)	$t_{1/2}$ (min)	c ($\times 10^{-3}$)
0.1	0.886	0.898	0.986	0.959	0.960	5.90	14.5	2.30
0.2	0.945	0.957	0.981	0.983	0.991	7.93	16.5	23.30
0.3	0.997	0.995	0.781	0.976	0.975	12.80	20.4	67.50
NaCl (M)	Zeroth order	First-order	Pseudo-second-order	Fickian	Parabolic diffusion			
					r^2	k ($\times 10^{-3}$) (mol-1L s-1)	$t_{1/2}$ (min)	c ($\times 10^{-3}$)
0.1	0.945	0.946	0.943	0.975	0.996	0.66	14.8	0.13
0.2	0.969	0.975	0.900	0.997	0.99	5.25	18.1	17.50
0.3	0.846	0.874	0.900	0.953	0.977	13.90	16.4	52.40

Table 5
Correlation coefficients (r^2), rate constant (k) and half-life ($t_{1/2}$) of isoprocab release from ZLH-DS-ISO-CA nanocomposite into solutions (Na_3PO_4 , Na_2SO_4 , NaCl)

Na ₃ PO ₄ (M)	Zeroth order	First-order	Parabolic diffusion	Fickian	Pseudo-second-order			
					r^2	k ($\times 10^{-3}$) (mol-1L s-1)	$t_{1/2}$ (min)	c
0.1	0.975	0.996	0.935	0.841	0.996	2.61	220.9	1.88
0.2	0.924	0.998	0.94	0.837	0.991	2.75	219.4	2.33
0.3	0.872	0.971	0.971	0.919	0.995	4.37	207.6	1.97
Na ₂ SO ₄ (M)	Zeroth order	First-order	Parabolic diffusion	Fickian	Pseudo-second-order			
					r^2	k ($\times 10^{-3}$) (mol-1L s-1)	$t_{1/2}$ (min)	c
0.1	0.858	0.958	0.989	0.916	0.997	3.93	223.2	3.90
0.2	0.727	0.919	0.985	0.900	0.996	4.62	222.6	3.94
0.3	0.773	0.926	0.981	0.882	0.996	5.76	220.2	3.60
NaCl (M)	Zeroth order	First-order	Parabolic diffusion	Fickian	Pseudo-second-order			
					r^2	k ($\times 10^{-3}$) (mol-1L s-1)	$t_{1/2}$ (min)	c
0.1	0.936	0.962	0.975	0.851	0.999	3.77	234.9	1.68
0.2	0.831	0.902	0.987	0.883	0.997	7.61	230.3	2.22
0.3	0.813	0.857	0.983	0.939	0.994	17.61	220.2	2.70

1. Conclusion

In conclusion, the PXRD pattern showed high crystallinity of ZLH-DS-ISO-CA (19.8%) compared to ZLH-DS-ISO-CHIT (16.9%) nanocomposite. Meanwhile, the thermal analysis showed that the maximum temperature of ISO anion in ZLH-DS-ISO-CHIT nanocomposite was higher than the ZLH-DS-ISO-CA nanocomposite, which resulted in a higher coated percentage. Therefore, it could be concluded that chitosan gives protection to ISO anion than CA. The morphology analysis for both nanocomposites showed almost similar surface characteristics. It supported the successful coating of chitosan and CA on the surface of ZLH-DS-ISO-CHIT and ZLH-DS-ISO-CA nanocomposites. When compared to the ZLH-DS-ISO-CHIT and ZLH-DS-ISO-CA nanocomposites, the percentage of ISO anion release from the interlayer of ZLH-DS-ISO was substantially higher in all solutions. The ISO anion release from ZLH-DS-ISO-CHIT nanocomposite was found to be at a much slower rate than that of ZLH-DS-ISO-CA nanocomposite in all solutions. Therefore, it can be proposed that chitosan is the best coater for ZLH-DS-ISO nanocomposite compared to CA. The kinetic study of ISO anion release from ZLH-DS-ISO-CHIT nanocomposite into Na_3PO_4 solution was fitted with the first order, while the parabolic diffusion model best describes the release of the ISO anion in Na_2SO_4 and NaCl solutions. In the meantime, the kinetic study of the ISO anion released from ZLH-DS-ISO-CA nanocomposite into all three solutions demonstrates the release profile followed by the pseudo-second-order. To summarise, surface modification of ZLH-DS-ISO nanocomposite using chitosan and cellulose acetate as a coater is critical as a protective layer to sustain anionic pesticide release from their nanocomposite. This output can be fine-tuned for controlled release applications in plant cultivation.

Conflict of interest: None

Acknowledgement

This research was supported by Ministry of Education (MOE) through Fundamental Research Grant Scheme (FRGS/1/2018/STG01/UPSI/02/4). Zuhailimuna Muda thanks UPSI for all support for this research.

References

1. da Silva, B.L., et al., *Increased antibacterial activity of ZnO nanoparticles: Influence of size and surface modification*. Colloids and Surfaces B: Biointerfaces, 2019. **177**: p. 440-447. DOI: <https://doi.org/10.1016/j.colsurfb.2019.02.013>.
2. Zhu, N., et al., *Surface modification of magnetic iron oxide nanoparticles*. Nanomaterials, 2018. **8**(10): p. 810. DOI: <https://doi.org/10.3390/nano8100810>.
3. Mandal, N., et al., *Novel chitosan grafted zinc containing nanoclay polymer biocomposite (CZNCBPBC): Controlled release formulation (CRF) of Zn^{2+}* . Reactive and Functional Polymers, 2018. **127**: p. 55-66. DOI: <https://doi.org/10.1016/j.reactfunctpolym.2018.04.005>.
4. Kango, S., et al., *Surface modification of inorganic nanoparticles for development of organic-inorganic nanocomposites—A review*. Progress in Polymer Science, 2013. **38**(8): p. 1232-1261. DOI: <https://doi.org/10.1016/j.progpolymsci.2013.02.003>.
5. Khutoryanskiy, V.V., *Beyond PEGylation: alternative surface-modification of nanoparticles with mucus-inert biomaterials*. Advanced Drug Delivery Reviews, 2018. **124**: p. 140-149. DOI: <https://doi.org/10.1016/j.addr.2017.07.015>.
6. Ling, W., et al., *Synthesis, surface modification, and applications of magnetic iron oxide nanoparticles*. Journal of Materials Research, 2019. **34**(11): p. 1828-1844. DOI: <https://doi.org/10.1557/jmr.2019.129>.
7. Jennings, J.A., et al., *Chitosan coatings to control release and target tissues for therapeutic delivery*. Therapeutic Delivery, 2015. **6**(7): p. 855-871. DOI: <https://doi.org/10.4155/tde.15.31>.
8. Luo, Y., et al., *Solid lipid nanoparticles for oral drug delivery: Chitosan coating improves stability, controlled delivery, mucoadhesion and cellular uptake*. Carbohydrate polymers, 2015. **122**: p. 221-229. DOI: <https://doi.org/10.1016/j.carbpol.2014.12.084>.

9. El Zowalaty, M.E., et al., *The ability of streptomycin-loaded chitosan-coated magnetic nanocomposites to possess antimicrobial and antituberculosis activities*. International journal of nanomedicine, 2015. **10**: p. 3269. DOI: <https://doi.org/10.2147/IJN.S74469>.
10. Sowjanya, M., et al., *Polymers used in the designing of controlled drug delivery system*. Research Journal of Pharmacy and Technology, 2017. **10**(3): p. 903. DOI: <https://doi.org/10.5958/0974-360X.2017.00168.8>.
11. Sikder, A., et al., *Recent trends in advanced polymer materials in agriculture related applications*. ACS Applied Polymer Materials, 2021. **3**(3): p. 1203-1217. DOI: <https://doi.org/10.1021/acsapm.0c00982>.
12. Peng, H., et al., *A novel nanocomposite matrix based on graphene oxide and ferrocene-branched organically modified sol-gel/chitosan for biosensor application*. Journal of Solid State Electrochemistry, 2014. **18**(7): p. 1941-1949. DOI: <https://doi.org/10.1007/s10008-014-2415-1>.
13. Sung, Y.K. and S.W. Kim, *Recent advances in polymeric drug delivery systems*. Biomaterials Research, 2020. **24**(1): p. 1-12. DOI: <https://doi.org/10.1186/s40824-020-00190-7>.
14. Mahmoud, M.G., E.M. El Kady, and M.S. Asker, *Chitin, chitosan and glucan, properties and applications*. World Journal of Agriculture and Soil Science, 2019. **3**(1): p. 1-19. DOI: <https://doi.org/10.33552/WJASS.2019.03.000553>.
15. Davidson, D.W., M.S. Verma, and F.X. Gu, *Controlled root targeted delivery of fertilizer using an ionically crosslinked carboxymethyl cellulose hydrogel matrix*. SpringerPlus, 2013. **2**(1): p. 1-9. DOI: <https://doi.org/10.1186/2193-1801-2-318>.
16. Paramo, L.A., et al., *Nanoparticles in agroindustry: Applications, toxicity, challenges, and trends*. Nanomaterials, 2020. **10**(9): p. 1654. DOI: <https://doi.org/10.3390/nano10091654>.
17. Stulzer, H.K., et al., *Development of controlled release captopril granules coated with ethylcellulose and methylcellulose by fluid bed dryer*. Drug Delivery, 2008. **15**(1): p. 11-18. DOI: <https://doi.org/10.1080/10717540701827196>.
18. Nuruzzaman, M.D., et al., *Nanoencapsulation, nano-guard for pesticides: a new window for safe application*. Journal of agricultural and food chemistry, 2016. **64**(7): p. 1447-1483. DOI: <https://doi.org/10.1021/acs.jafc.5b05214>.
19. Elieh-Ali-Komi, D. and M.R. Hamblin, *Chitin and chitosan: production and application of versatile biomedical nanomaterials*. International journal of advanced research, 2016. **4**(3): p. 411.
20. Joseph, S.M., et al., *A review on source-specific chemistry, functionality, and applications of chitin and chitosan*. Carbohydrate Polymer Technologies and Applications, 2021. **2**: p. 100036. DOI: <https://doi.org/10.1016/j.carpta.2021.100036>.
21. Yuan, Q., et al., *Controlled and extended drug release behavior of chitosan-based nanoparticle carrier*. Acta biomaterialia, 2010. **6**(3): p. 1140-1148. DOI: <https://doi.org/10.1016/j.actbio.2009.08.027>.
22. Kashyap, P.L., X. Xiang, and P. Heiden, *Chitosan nanoparticle based delivery systems for sustainable agriculture*. International journal of biological macromolecules, 2015. **77**: p. 36-51. DOI: <https://doi.org/10.1016/j.jbiomac.2015.02.039>.
23. Jiménez-Gómez, C.P. and J.A. Cecilia, *Chitosan: a natural biopolymer with a wide and varied range of applications*. Molecules, 2020. **25**(17): p. 3981. DOI: <https://doi.org/10.3390/molecules25173981>.
24. Vroman, I. and L. Tighzert, *Biodegradable polymers*. Materials, 2009. **2**(2): p. 307-344. DOI: <https://doi.org/10.3390/ma2020307>.
25. Lawrenciana, D., et al., *Controlled release fertilizers: A review on coating materials and mechanism of release*. Plants, 2021. **10**(2): p. 238. DOI: <https://doi.org/10.3390/plants10020238>.
26. Senna, A.M., et al., *Synthesis, characterization and application of hydrogel derived from cellulose acetate as a substrate for slow-release NPK fertilizer and water retention in soil*. Journal of Environmental Chemical Engineering, 2015. **3**(2): p. 996-1002. DOI: <https://doi.org/10.1016/j.jece.2015.03.008>.
27. Ahmad, M.S., et al., *Electrochemical detection of hydroquinone by square wave voltammetry using a Zn layered hydroxide-ferulate (ZLH-F) modified MWCNT paste electrode*. Int. J. Electrochem. Sci, 2018. **13**: p. 373-383. DOI: <https://doi.org/10.20964/2018.01.31>.
28. Beecroft, L.L. and C.K. Ober, *Nanocomposite materials for optical applications*. Chemistry of materials, 1997. **9**(6): p. 1302-1317. DOI: <https://doi.org/10.1021/cm960441a>.
29. Hashim, N., et al., *Development of a novel nanocomposite consisting of 3-(4-methoxyphenyl) propionic acid and magnesium layered hydroxide for controlled-release formulation*. Journal of Experimental Nanoscience, 2016. **11**(10): p. 776-797. DOI: <https://doi.org/10.1080/17458080.2016.1171916>.

30. dos Santos Silva, M., et al., *Paraquat-loaded alginate/chitosan nanoparticles: preparation, characterization and soil sorption studies*. Journal of hazardous materials, 2011. **190**(1-3): p. 366-374.DOI: <https://doi.org/10.1016/j.jhazmat.2011.03.057>.
31. Lerner, D.A., et al., *Synthesis and Properties of New Multilayer Chitosan@ layered Double Hydroxide/Drug Loaded Phospholipid Bilayer Nanocomposite Bio-Hybrids*. Materials, 2020. **13**(16): p. 3565.DOI: <https://doi.org/10.3390/ma13163565>.
32. Kujawa, J., et al., *Preparation and characterization of cellulose acetate propionate films functionalized with reactive ionic liquids*. Polymers, 2019. **11**(7): p. 1217.DOI: <https://doi.org/10.3390/polym11071217>.
33. Sutrisna, P.D., et al. *ZIF-8/Cellulose Acetate Based Mixed Matrix Membranes (MMMs) Synthesis and Characterization*. Trans Tech Publ.DOI: <https://doi.org/10.4028/www.scientific.net/AST.104.57>.
34. Bhuyan, P., et al., *Understanding the chemistry and sources of precipitation ions in the mid-Brahmaputra valley of northeastern India*. Aerosol and Air Quality Research, 2020. **20**(12): p. 2690-2704.DOI: <https://doi.org/10.4209/aaqr.2020.02.0072>.
35. Al Ali, S.H.H., et al., *Preparation of hippurate-zinc layered hydroxide nanohybrid and its synergistic effect with tamoxifen on HepG2 cell lines*. International Journal of Nanomedicine, 2011. **6**: p. 3099.DOI: <https://doi.org/10.2147/IJN.S24510>.
36. Cursino, A.C.T., et al., *Rare earth and zinc layered hydroxide salts intercalated with the 2-aminobenzoate anion as organic luminescent sensitizer*. Materials Research Bulletin, 2015. **70**: p. 336-342.DOI: <https://doi.org/10.1016/j.materresbull.2015.04.055>.
37. Ruiz, C.V., M.E. Becerra, and O. Giraldo, *Structural, thermal, and release properties of hybrid materials based on layered zinc hydroxide and caffeic acid*. Nanomaterials, 2020. **10**(1): p. 163.DOI: <https://doi.org/10.3390/nano10010163>.
38. Badawy, M.E.I. and E.I. Rabea, *Chitosan-based edible membranes for food packaging*, in *Bio-based Materials for Food Packaging*. 2018, Springer. p. 237-267.DOI: https://doi.org/10.1007/978-981-13-1909-9_11.
39. Elhefian, E.A., M.M. Nasef, and A.H. Yahaya, *Preparation and characterization of chitosan/agar blended films: part 2. Thermal, mechanical, and surface properties*. E-Journal of Chemistry, 2012. **9**(2): p. 510-516.DOI: <https://doi.org/10.1155/2012/285318>.
40. Demel, J., et al., *Insight into the structure of layered zinc hydroxide salts intercalated with dodecyl sulfate anions*. The Journal of Physical Chemistry C, 2014. **118**(46): p. 27131-27141.DOI: <https://doi.org/10.1021/jp508499g>.
41. Barahuie, F., et al., *Sustained release of anticancer agent phytic acid from its chitosan-coated magnetic nanoparticles for drug-delivery system*. International journal of nanomedicine, 2017. **12**: p. 2361.DOI: <https://doi.org/10.2147/IJN.S126245>.
42. Verma P, et al., *Molecular Structure, Spectral Investigations, Hydrogen Bonding Interactions and Reactivity-Property Relationship of Caffeine-Citric Acid Cocrystal by Experimental and DFT Approach* Front. Chem. 9 708538. 2021.DOI: <https://doi.org/10.3389/fchem.2021.708538>.
43. Gadwal, I., *A brief overview on preparation of self-healing polymers and coatings via hydrogen bonding interactions*. Macromol, 2021. **1**(1): p. 18-36.DOI: <https://doi.org/10.3390/macromol1010003>.
44. Kura, A.U., et al., *Preparation of Tween 80-Zn/Al-levodopa-layered double hydroxides nanocomposite for drug delivery system*. The Scientific World Journal, 2014. **2014**.DOI: <https://doi.org/10.1155/2014/104246>.
45. Wei, P.-R., et al., *Synthesis and characterization of chitosan-coated near-infrared (nir) layered double hydroxide-indocyanine green nanocomposites for potential applications in photodynamic therapy*. International journal of molecular sciences, 2015. **16**(9): p. 20943-20968.DOI: <https://doi.org/10.3390/ijms160920943>.
46. Sato, R., et al., *Intercalation of a Cationic Cyanine Dye Assisted by Anionic Surfactants within Mg-Al Layered Double Hydroxide*. ACS omega, 2021. **6**(37): p. 23837-23845.DOI: <https://doi.org/10.1021/acsomega.1c02724>.
47. Ghamami, S., M. Golzani, and A. Lashgari, *New inorganic-based nanohybrids of layered zinc hydroxide/Parkinson's disease drug and its chitosan biopolymer nanocarriers with controlled release rate*. Journal of Inclusion Phenomena and Macrocyclic Chemistry, 2016. **86**(1): p. 67-78.DOI: <https://doi.org/10.1007/s10847-016-0642-z>.
48. Gomez, N.A.G. and F. Wypych, *Nanocomposites of polyethylene and ternary (Mg+ Zn/Al) layered double hydroxide modified with an organic UV absorber*. Journal of Polymer Research, 2019. **26**(8): p. 1-10.DOI: <https://doi.org/10.1007/s10965-019-1868-4>.

49. Barkhordari, S. and M. Yadollahi, *Carboxymethyl cellulose capsulated layered double hydroxides/drug nanohybrids for Cephalexin oral delivery*. Applied Clay Science, 2016. **121**: p. 77-85. DOI: <https://doi.org/10.1016/j.clay.2015.12.026>.
50. Virkar, S., *characterization of nanocomposites based on polyethylene and Mg-Al layered double hydroxide with intercalated compounds*. Adv. Mater. Sci. Appl, 2014. **3**: p. 150-156. DOI: <https://doi.org/10.5963/AMSA0303006>.
51. Biswick, T., D.-H. Park, and J.-H. Choy, *Enhancing the UV A1 screening ability of caffeic acid by encapsulation in layered basic zinc hydroxide matrix*. Journal of Physics and Chemistry of Solids, 2012. **73**(12): p. 1510-1513. DOI: <https://doi.org/10.1016/j.jpics.2011.11.039>.
52. Lee, J.W., W.C. Choi, and J.-D. Kim, *Size-controlled layered zinc hydroxide intercalated with dodecyl sulfate: effect of alcohol type on dodecyl sulfate template*. CrystEngComm, 2010. **12**(10): p. 3249-3254. DOI: <https://doi.org/10.1039/c002296a>.
53. Hussein, M.Z., et al., *Synthesis and characterization of [4-(2, 4-dichlorophenoxybutyrate)-zinc layered hydroxide] nanohybrid*. Solid State Sciences, 2010. **12**(5): p. 770-775. DOI: <https://doi.org/10.2147/IJN.S53079>.
54. Ramimoghadam, D., M.Z.B. Hussein, and Y.H. Taufiq-Yap, *The effect of sodium dodecyl sulfate (SDS) and cetyltrimethylammonium bromide (CTAB) on the properties of ZnO synthesized by hydrothermal method*. International journal of molecular sciences, 2012. **13**(10): p. 13275-13293. DOI: <https://doi.org/10.3390/ijms131013275>.
55. Hussein-Al-Ali, S.H., et al., *Synthesis, characterization, controlled release, and antibacterial studies of a novel streptomycin chitosan magnetic nanoantibiotic*. International journal of nanomedicine, 2014. **9**: p. 549. DOI: <https://doi.org/10.1016/j.solidstatesciences.2010.02.022>.
56. Zhou, C.-H., et al., *like composites of cellulose acetate–organo-montmorillonite for removal of hazardous anionic dye in water*. Chemical Engineering Journal, 2012. **209**: p. 223-234. DOI: <https://doi.org/10.1016/j.cej.2012.07.107>.
57. Deshmukh, K., et al., *Newly developed biodegradable polymer nanocomposites of cellulose acetate and Al₂O₃ nanoparticles with enhanced dielectric performance for embedded passive applications*. Journal of Materials Science: Materials in Electronics, 2017. **28**(1): p. 973-986. DOI: <https://doi.org/10.1007/s10854-016-5616-9>.
58. Qian, L. and H. Zhang, *Green synthesis of chitosan-based nanofibers and their applications*. Green Chemistry, 2010. **12**(7): p. 1207-1214. DOI: <https://doi.org/10.1039/b927125b>.
59. Abdul Latip, A.F., et al., *Release behavior and toxicity profiles towards A549 cell lines of ciprofloxacin from its layered zinc hydroxide intercalation compound*. Chemistry Central Journal, 2013. **7**(1): p. 1-11. DOI: <https://doi.org/10.1186/1752-153X-7-119>.
60. Li, M., et al., *Layered double hydroxide/chitosan nanocomposite beads as sorbents for selenium oxoanions*. Industrial & Engineering Chemistry Research, 2018. **57**(14): p. 4978-4987. DOI: <https://doi.org/10.1021/acs.iecr.8b00466>.
61. Wang, J., H. Jiang, and N. Jiang, *Study on the pyrolysis of phenol-formaldehyde (PF) resin and modified PF resin*. Thermochimica Acta, 2009. **496**(1-2): p. 136-142. DOI: <https://doi.org/10.1016/j.tca.2009.07.012>.
62. De, S., S. Mohanty, and S.K. Nayak, *Structure-property relationship of layered metal oxide phosphonate/chitosan nanohybrids for transducer in biosensing device*. Journal of Materials Engineering and Performance, 2015. **24**(1): p. 114-127. DOI: <https://doi.org/10.1007/s11665-014-1293-0>.
63. Tan, J.M., et al., *Incorporation of levodopa into biopolymer coatings based on carboxylated carbon nanotubes for pH-dependent sustained release drug delivery*. Nanomaterials, 2018. **8**(6): p. 389. DOI: <https://doi.org/10.3390/nano8060389>.
64. Romero, R.B., C.A.P. Leite, and M. do Carmo Gonçalves, *The effect of the solvent on the morphology of cellulose acetate/montmorillonite nanocomposites*. Polymer, 2009. **50**(1): p. 161-170. DOI: <https://doi.org/10.1016/j.polymer.2008.10.059>.
65. Mohana Raju, K. and M. Padmanabha Raju, *Synthesis of novel superabsorbing copolymers for agricultural and horticultural applications*. Polymer international, 2001. **50**(8): p. 946-951. DOI: <https://doi.org/10.1002/pi.721>.
66. Zhang, J.P., A. Li, and A.Q. Wang, *Study on superabsorbent composite. V. Synthesis, swelling behaviors and application of poly (acrylic acid-co-acrylamide)/sodium humate/attapulgit superabsorbent composite*. Polymers for advanced technologies, 2005. **16**(11-12): p. 813-820. DOI: <https://doi.org/10.1002/pat.657>.
67. Kong, X., et al., *Preparation of Glycy-L-Tyrosine intercalated layered double hydroxide film and its in vitro release behavior*. Chemical Engineering Journal, 2010. **157**(2-3): p. 598-604. DOI: <https://doi.org/10.1016/j.cej.2010.01.016>.

68. Parida, U.K., et al., *Synthesis and characterization of chitosan-polyvinyl alcohol blended with cloisite 30B for controlled release of the anticancer drug curcumin*. Journal of Biomaterials and Nanobiotechnology, 2011. **2**(04): p. 414. DOI: <https://doi.org/10.4236/jbnt.2011.24051>.
69. Khan, S.B., et al., *Controlled release of organic-inorganic nanohybrid: cefadroxil intercalated Zn-Al-layered double hydroxide*. International journal of nanomedicine, 2018. **13**: p. 3203. DOI: <https://doi.org/10.2147/IJN.S138840>.
70. Strimaite, M., et al., *Layered terbium hydroxides for simultaneous drug delivery and imaging*. Dalton Transactions, 2021. **50**(29): p. 10275-10290. DOI: <https://doi.org/10.1039/D1DT01251G>.
71. Hashim, N., et al., *Synthesis and controlled release of cloprop herbicides from cloprop-layered double hydroxide and cloprop-zinc-layered hydroxide nanocomposites*. Open Journal of Inorganic Chemistry, 2014. **2014**. DOI: <https://doi.org/10.4236/ojic.2014.41001>.
72. Hashim, N., et al., *Release behavior of dichlorprop from Zn/Al-ldh-dichlorprop nanocomposite into chloride, carbonate and phosphate solutions*. Jurnal Teknologi, 2019. **81**(2). DOI: <https://doi.org/10.11113/jt.v81.12919>.
73. Hua, S., et al., *Controlled release of ofloxacin from chitosan-montmorillonite hydrogel*. Applied Clay Science, 2010. **50**(1): p. 112-117. DOI: <https://doi.org/10.1016/j.clay.2010.07.012>.
74. Ayawei, N., et al., *Synthesis, characterization and application of Mg/Al layered double hydroxide for the degradation of congo red in aqueous solution*. Open Journal of Physical Chemistry, 2015. **5**(03): p. 56. DOI: <https://doi.org/10.4236/ojpc.2015.53007>.
75. Usman, M.S., et al., *Synthesis and characterization of protocatechuic acid-loaded gadolinium-layered double hydroxide and gold nanocomposite for theranostic application*. Applied Nanoscience, 2018. **8**(5): p. 973-986. DOI: <https://doi.org/10.1007/s13204-018-0752-6>.
76. Devesa-Rey, R., et al., *Preparation of Synthetic Clays to Remove Phosphates and Ibuprofen in Water*. Water, 2021. **13**(17): p. 2394. DOI: <https://doi.org/10.3390/w13172394>.
77. Smith, R.B., E. Khoo, and M.Z. Bazant, *Intercalation kinetics in multiphase-layered materials*. The Journal of Physical Chemistry C, 2017. **121**(23): p. 12505-12523. DOI: <https://doi.org/10.1021/acs.jpcc.7b00185>.
78. Komarala, E.P., et al., *Studies on drug release kinetics and antibacterial activity against drug-resistant bacteria of cefotaxime sodium loaded layered double hydroxide-fenugreek nanohybrid*. New Journal of Chemistry, 2018. **42**(1): p. 129-136. DOI: <https://doi.org/10.1039/C7NJ03622A>.
79. Ahmad, R., et al., *Synthesis and characteristics of valeric acid-zinc layered hydroxide intercalation material for insect pheromone controlled release formulation*. Journal of Materials, 2016. **2016**(s1285721). DOI: <https://doi.org/10.1155/2016/1285721>.
80. Ahmad, R., et al., *Evaluation of controlled-release property and phytotoxicity effect of insect pheromone zinc-layered hydroxide nanohybrid intercalated with hexenoic acid*. Journal of agricultural and food chemistry, 2015. **63**(51): p. 10893-10902. DOI: <https://doi.org/10.1021/acs.jafc.5b03102>.
81. Theiss, F.L., et al., *A review of the removal of anions and oxyanions of the halogen elements from aqueous solution by layered double hydroxides*. Journal of colloid and interface science, 2014. **417**: p. 356-368. DOI: <https://doi.org/10.1016/j.jcis.2013.11.040>.